Powder Technology 270 (2015) 393–410

Contents lists available at ScienceDirect

Powder Technology

journal homepage: www.elsevier.com/locate/powtec

# Comparative analysis of empirical descriptions of eccentric flow in silo model by the linear and nonlinear regressions

Irena Sielamowicz [a,*], Artur Czech [b], Tomasz A. Kowalewski [c]

[a] University of Zielona Góra, 65-516 Zielona Góra, Prof. Z. Szafrana 1, Poland
[b] Bialystok University of Technology, Wiejska 45 A, Bialystok, Poland
[c] Institute of Fundamental Technological Research, Polish Academy of Sciences, Pawińskiego 5B, Warsaw, Poland

ARTICLE INFO

*Article history:*
Received 9 June 2014
Received in revised form 29 September 2014
Accepted 3 October 2014
Available online 14 October 2014

*Keywords:*
Eccentric granular flow
Silo model
Empirical description
Linear and nonlinear regression
Gaussian description
Double logarithm

ABSTRACT

This paper is a third of a series of the three where eccentric cases of flow in silo models recorded by the DPIV technique are presented and discussed in detail. The methodology of empirical descriptions of velocities, flow rate and stagnant zone boundaries on the base of registered velocity fields in eccentric filling and discharge in 2D silo model was discussed. In previous two papers [1,2] we analyzed also eccentric flows but with different locations of the outlet. It was stated that in practice even tiny eccentricity of filling or discharge processes may lead to quite an unexpected behavior of the silo structure. During asymmetrical processes, flow patterns and wall stresses may be quite different. It is therefore crucial to identify how flow patterns developed in the material during eccentric filling or discharge and to determine both the flow rate and wall stresses occurring under such state of loads. Thus, we discuss here the third case of discharge — located in the center of the silo bottom. A comparison of these three cases of discharge mode will be presented in the next paper. Empirical descriptions of eccentric flow velocities in silo model by the linear and nonlinear regressions are presented here with specific functions like the Gaussian function and "the double logarithmic function". In both methods the velocity was also descripted by linearization and in the Gaussian method also by the nonlinear method of Gauss–Newton and in the case of the method of double logarithm — the nonlinear method of Levenberg–Marquardt was applied. Velocities were predicted by using interpolation due to the nonlinear model of the Gaussian type and to the nonlinear function of "the double logarithm".



## 1. Literature review

Eccentricity is always a dangerous factor influencing to the silo structure. Technological processes can be disrupted while any eccentricity occurred. International Standards usually relate to axial symmetric states of stresses and even avoid defining discharge pressures and flow patterns because of continuing uncertainties defining the flow channel geometry and wall pressures under eccentric discharge or the values of increased coefficients of horizontal pressure during eccentric discharge [3,4]. In [3–6] we read comments on the eccentricity of the outlet, on the flow channel geometry and the wall pressure under eccentric discharge. Eccentric discharge is described as a flow pattern in the stored solid arising from moving solid being asymmetrically distributed relative to the vertical centreline of the silo. This normally arises as a result of an eccentrically located outlet but can be caused by other asymmetrical phenomena which are not clearly defined. As it was commented in [1] calculations for flow channel geometry are required for only one size of flow channel contact with the wall, which should be determined for $\Theta_C = 35^\circ$ and wall pressures under eccentric discharge are also defined and discussed in [1]. Researchers tried to make approaches to develop designing of bins under eccentric discharge [7–9] and Carson [10] in detail presented the issue of eccentricity as one of the major causes of hopper failures. Eccentricity of the flow to the silo axis causes the pressure patterns to become much more complex than in centric cases. In the field of silo investigations three main issues are usually analyzed: pressures under eccentric discharge, flow patterns and stagnant zone boundaries.

Works on eccentric discharge have been published for many years and a few researchers have dealt with this complicated problem. In [1] one can find a detail discussion of investigations in silos during eccentric discharge, silo loads and wall loads, measurements of wall loads when unloaded eccentrically, the effect of eccentric unloading in a model bin for different unloading rates, the effect of eccentricity and ways of discharge in silo, flow patterns in a silo with symmetrical and eccentric outlet. There are works [7–13] where authors investigated the behavior of silos under eccentric discharge, identified flow patterns and stresses on the wall during centric and eccentric discharges. They also made measurements of the wall pressures under eccentric discharge, investigated discharge and the eccentricity of the hopper influence on silo wall pressures, and measured experimentally the heights of the stagnant

* Corresponding author.
*E-mail addresses:* irena.sielamowicz@gmail.com (I. Sielamowicz), a.czech@pb.edu.pl (A. Czech), tkowale@ippt.gov.pl (T.A. Kowalewski).

http://dx.doi.org/10.1016/j.powtec.2014.10.007
0032-5910/

zones for two kinds of granular materials after hopper eccentric and centric discharges. Theoretical analyses were made using the kinematic model, proposed by Nedderman and Tüzün [10,13,14], for filling and discharge — centrally and eccentrically. Further numerical investigations were conducted in [15,16] by applying FEM modeling in the analysis of influence of hopper eccentricity on wall pressures or a buckling strength of steel silo subject to code specified pressures for eccentric discharge. Another field of investigations was related to localized deformation pattern in granular materials, investigating shear localizations in granular materials numerically and compared the obtained results to experimental data [17]. In [18] one can find a long list of references concerning investigation of eccentric discharge.

Investigation of flow patterns and wall stresses in silos and other hoppers is usually carried out on laboratory models. Many different measurement techniques have been used in such studies: visual measurements through transparent walls, colored layers and photography, colored layers and dissection after freezing the flow with paraffin wax, photographic or video techniques, and tracer techniques using X-rays and radio pills and insertion of markers to measure residence times [18]. In laboratory tests very significant scale effects in silo flow and pressures were reported in [19–23]. However, almost all of these techniques are not viable at full scale. Many tests on full scale silos were made to measure wall pressures [24]. There are a few examples given in literature where the measurements of flow patterns were performed on line [18,25,26]. Such investigations are very expensive, due not only to the enormous size of the silo but also to the difficulties in accessing the structure. Because of the difficulties of access at natural scale such as opaque walls, opaque solids, surface covered with dust and intrusive investigation techniques, such as the penetration of the wall, rarely acceptable by silo owners, model silo studies seem to be very useful in the recognizing flow patterns. Though, the challenge of observing flow processes at full scale remains considerable. The flow inside the silo has been poorly identified till today and the investigation of flow modes inside the silo is almost impossible.

Silos are structures having round horizontal cross sections. Usually all laboratory models are flat and only flat flow is investigated. There are also round laboratory models but in this case, it is much more difficult to measure stagnant zone boundaries. In such models usually the problem of flow modes and determining wall pressures are made.

## 2. Experimental procedure

To register velocities of flowing grains we applied the DPIV (Digital Particle Image Velocimetry) technique which made it possible to identify the eccentric flow in the plane flat-bottomed model silo made of Plexiglas. Two other eccentric cases of the flow were discussed in [1,2]. The images of the flowing material were recorded by a high-resolution camera and evaluated using the DPIV technique. The adopted DPIV technique was based on the optical flow algorithm, which has been found to be most reliable for granular flow images. In [43] the authors presented a detailed description of the OF-DPIV, including its development and application. The experimental setup used for the flow analysis consisted of a transparent acrylic plastic box, a set of illumination lamps, and a high-speed CCD camera (PCO1200HS) with an objective 50 mm lens produced by PCO AG, Kelheim, Germany [http://www.pco.de/high-speed-cameras/pco1200-hs/]. The transparent flat-bottom silo model had a height 800 mm, a depth of 100 mm and a width of 260 mm. The model was placed on a stand and granular material was supplied through a box suspended above the model. The bottom of the supplying box contained a sieve and the box was filled with flax seeds to 2/3 of its height. The model was filled close to the left wall. The discharge outlet was located centrally at the bottom of the silo. The width of the outlet was 10 mm. In order to evaluate transient velocity fields, long sequences of 100–400 images were taken at variable time intervals, covering the whole of the discharge time. The DPIV technique used here produced velocity fields for the full interrogation area. The velocity profiles obtained inside the quasi two-dimensional silo were smooth and free of shock-like discontinuities. The flax seeds showed some effects of static electricity when flowing and sliding over the transparent acrylic plastic. The granular material was introduced in a form of a uniform stream into the silo model to obtain uniform and repeatable packing of the material with no particle segregation. The evolution of the flow region and the traces of flowing particles were evaluated from recorded images. Pairs of digital short exposure images were taken to describe how the velocity field varies in the flowing material. This data was used in empirical description of the flow. The properties of the amaranth seed used in the experiments were: wall friction against transparent Plexiglas $\varphi_w = 26°$, angle of internal friction $\varphi_e = 25°$ granular material density deposited through a pipe with zero free-fall 746 kg/m$^3$ at 1 kPa and 747 kg/m$^3$ at 8 kPa, Young's modulus 6.11 MPa. The values of the angle of internal friction for the flax-seed are taken from the Polish Standard PN-89/B-03262. Sequences of 12-bit images with the resolution of $1280 \times 1024$ pixels were acquired by Pentium 4 based personal computer using IEEE1394 interface. The system allowed acquiring up to 1000 images at time interval of 1.5 ms (667 fps). The velocity field was evaluated for triplets of images using the DPIV based on the Optical Flow technique. Dense velocity fields with vectors for each pixel of the image were obtained and used for further evaluation of the velocity profiles, velocity contours and streamlines. The term “streamline” is defined as a direction of the flow of different particles at the same time. Intrinsic resolution of the PIV technique is limited by the size of the area of interest that is used in the application of the cross correlation algorithm between subsequent images and this is generally one order of magnitude larger than a single pixel. The aim of the present investigation is to explore the possibility of using the Optical Flow technique based on PIV in measuring granular material flow velocity. In granular material flow one usually visualizes a track of individual particles, not necessarily coinciding with the streamline. Such tracks were obtained by Choi et al. [11], who used a high-speed imaging technique to trace the position of single particles in granular materials. Velocity profiles obtained that way for the flow of granular material inside a quasi-two-bottomed silo were smooth and free of shock-like discontinuities. In contrast, the DPIV technique used here produces velocity field for the full interrogation area, and this can be used to predict the natural track of individual particles.

In general, this technique was applied in fluid mechanics and its first applications to granular material flow were presented by [27,28]. One of the first successful attempts to apply the PIV technique to granular matter was described in [28–35] and reported the use of the PIV technique in their experiments to obtain information on local velocities of particles at several elevations in densely packed materials. Ostendorf and Schwedes in [30] combined PIV measurements with wall normal stress measurements at different points of time in a large scale silo.

Observations of the discharge process allow us to understand the behavior of the flowing material. As mentioned above, different measurement techniques have been used in investigations of flow in silo models. A number of experimental works have been focused to measure flow patterns. Optical techniques are commonly used in the analysis of velocity profiles near the transparent silo walls. The X-ray technique was frequently applied to obtain information from deeper flow layers [36,37]. Also, other non-invasive measurement techniques were applied to register granular flow, density and velocity fields in flowing zones, among others spy-holes, radio transmitters, positron emission [38], magnetic resonance imaging, radioactive tracers, and ultrasonic speckle velocimetry. More details on different techniques used in investigations of granular flow in small models can be found in references given in [28,38–42].

The case discussed here is recognized as eccentric filling but the position of the outlet that was symmetrically located was shown in Fig. 1. This location of the outlet produces a very interesting flow mode of the material, becoming symmetrical very quickly after opening the outlet. Despite eccentric feeding, just after 25th of the flow, the material

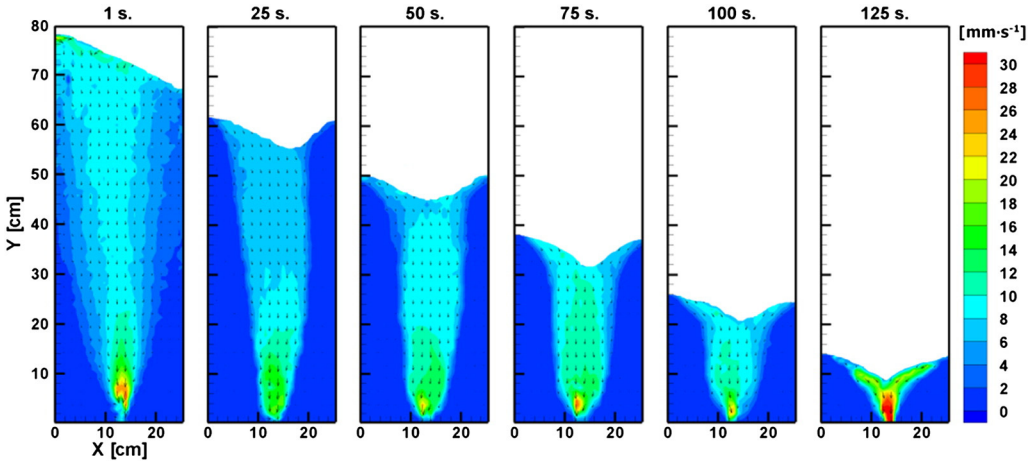


**Fig. 1.** Velocity distributions in the model while eccentric filling on the left and discharge in the center [34].

tends to form a symmetric flow. Soon after the initiation it is possible to observe nearly uniform flow channel for the entire height of the silo. In the plug flow region the velocity vectors in the initial phase of the flow are still not vertical but soon they pass directly and vertically to the outlet. In the upper part of the flow the velocity vectors indicate converging lateral flow towards the flowing zone. It seems that the central outlet induced the formation of the central plug flow.

The technique DPIV provides wide possibilities to obtain various data on the flow. We present velocity distributions on the various levels in the model (cf. Fig. 2). The profiles of vertical velocity components across the cavity were obtained at different heights indicated in the legend in Fig. 2 and at time steps of 1 s, 25 s, 50 s, 75 s, and 100 s after the beginning of the experiment. In Fig. 2a, at $h = 5$ cm above the outlet (the red line) one can observe the shape of the velocity profile. This profile is a special one because in each case of eccentric flow it behaves individually especially at the beginning of the flow [1,2]. It means that the central position of the outlet makes the flow symmetric soon after the flow starts. The filling feed does not play a significant role. The other profiles form a bunch of functions on the due levels. In the case of central discharge, this velocity profile reaches its maximum value in the flowing zone and becomes symmetric. Fig. 3 presents an evolution in time of the stagnant zone boundaries for three eccentric cases.

Three analyzed eccentric flows are very complex, especially due to appearance of localisation of deformation between flowing and stationary solid. Very narrow zones occur between flowing and stagnant material. These narrow zones are of intense shearing. Our investigation was performed in the model with smooth walls thus the shear zones do not form close to the wall. They can also occur between the wall and the stagnant material but in the case when the wall is rough. The registered deformation fields in the flowing flax seed in the plane model during eccentric flow and obtained directions of deformation provided valuable information on the mechanism of the granular behavior inside the silo. The knowledge of the range of deformation fields is the reason to perform theoretical description of shear localisation in flow processes. And this can be presented in our future works.

## 3. Experimental results and statistical descriptions

The main objective of this paper is to present statistical analysis of experimental results obtained in the eccentric flow case and searching for empirical description relating to experimental readings.

### 3.1. Results of velocity $V_y$ for time instants $t = 1, 25, 50, 75$ s

Results of experimental measurements of velocity $V_{y_i}$ for level $h = 5$, 10, 20, 30, 40 cm and for time instants $t = 1$, 25, 50, 75 s are given in Tables A–E in the Appendix.

### 3.2. Rejection of "thick errors"

On the base of data given in Tables A–E (given in the Appendix) we calculate the average vertical velocity $\overline{V}_y$ for different localizations of points $x$ and the standard deviation $S$ using the formula:

$$\overline{V}_y = \sum_{i=1}^{n} \frac{V_{y_i}}{n}$$
$$S = \sqrt{\frac{\sum_{i=1}^{n}\left(V_{y_i} - \overline{V}_y\right)^2}{n}} \tag{1}$$

where: $\overline{V}_y$ denotes the average values of velocities, $V_{y_i}$ is the flow velocity mm/s, $n$ is the number of time instants taken for the analysis and $S$ is the standard deviation.

One of the methods, how to estimate the presence of so called "thick" errors in our experimental data, is to calculate statistics $K$ according to formula (2):

$$K = \frac{\left|V_{y_i} - \overline{V_y}\right| \max}{S}. \tag{2}$$

Values of statistics $K$ are calculated on the base of data given in Tables A–E in the Appendix. The critical value of this statistics $K_{crit}$ for the significance level $\alpha = 0.05$ will be taken from [44]. If the value of statistics $K$ is lower than the critical value $K_{crit}$ then we do not have any reason to think that so called "thick" errors exist in our experimental data. And vice versa, if the value of the statistics exceeds the critical value $K_{crit}$ then we should reject such experimental readings.

### 3.3. Investigation of influence of time on velocity of flowing grains in the model

On the base of data given in Tables A–E presented in the Appendix, the confidence intervals for average values of velocities were calculated according to formula:

$$\overline{V}_y - t_{n-1,\,1-\frac{\alpha}{2}} \frac{S}{\sqrt{n-1}} < \mu < \overline{V}_y + t_{n-1,\,1-\frac{\alpha}{2}} \frac{S}{\sqrt{n-1}} \tag{3}$$

where: $\overline{V}_y$ and $S$ were calculated according to formula (1), $t_{n-1,1-\alpha/2}$ is the quantile of $t$-Student distribution for significance level $\alpha = 0.05$ [44], and $\mu$ denotes the average value of population for $n - 1$ numbers of freedom.

The calculations presented above are given in Tables F–J in the Appendix.

Comparing data given in Tables A–E with data given in Tables F–J presented in the Appendix we can state, that there is no reason to reject "zero hypothesis", that means that time is not an important factor influencing on the velocity for any given point *x*.

### 3.4. Investigation of velocity values for points located symmetrical to the silo symmetry axis

The axis of symmetry of the silo model is located in the distance at $x = 13$ cm from the lateral edge of the model. Symmetrical locations of points are for abscissa $13 - n_i$ and $13 + n_i$, where $n_i$ is the readings of velocities for points located on both sides of the axis of symmetry of the silo model.

We assume "the zero hypothesis" ($H$) and "the opposite hypothesis" ($H_1$):

$$H : \mu_{13-n_i} = \mu_{13+n_i},\quad H_1 : \mu_{13-n_i} \neq \mu_{13+n_i}$$

and in this way we verify the hypothesis of the average value of two populations. To do this we calculate statistics $t$ in the case of the same number of repetitions:

$$t = \frac{\left|\overline{X}_{13-n_i} - \overline{X}_{13+n_i}\right|}{\sqrt{S^2_{13-n_i} + S^2_{13+n_i}}}\sqrt{n-1} \tag{4}$$

or in the case of different numbers of repetitions of experiments by formula (5):

$$t = \frac{\left|\overline{X}_{13-n_i} - \overline{X}_{13+n_i}\right|}{\sqrt{n_{13-n_i}S^2_{13-n_i} + n_{13+n_i}S^2_{13+n_i}}}\sqrt{\frac{n_{13-n_i}n_{13+n_i}\left(n_{13-n_i} + n_{13+n_i} - 2\right)}{n_{13-n_i} + n_{13+n_i}}}. \tag{5}$$

The critical value in this case at the level of significance $\alpha = 0.05$ according to the t-Student is $t_{critical} = t_{0.05;13-n_i\,,13+n_i}$.

In this case when the value of statistics calculated from formula (4) to (5) is higher than the critical value then the hypothesis $H$ should be rejected, in the opposite case there is no reason to reject the hypothesis.

Before calculating formulas (4) and (5), we have found the homogeneity of the variance for various heights $h$ in the model using the

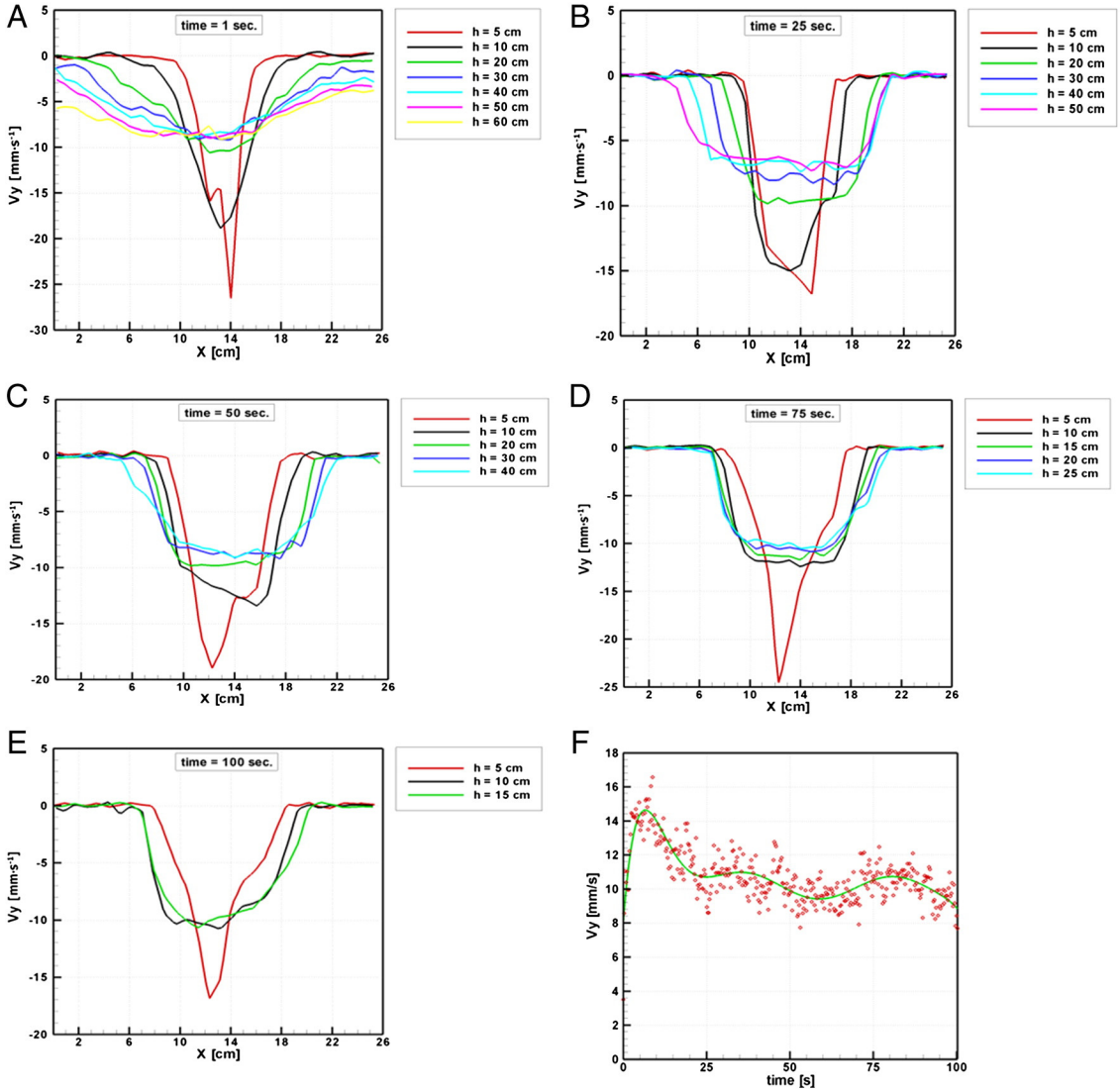


**Fig. 2.** A–E) Velocity profiles for the flow of flax-seed obtained for A) eccentric filling on the left and discharge in the central part of the bottom; F) variation of velocity–distribution in time, G–J) velocity profiles on selected levels inside the model [34].

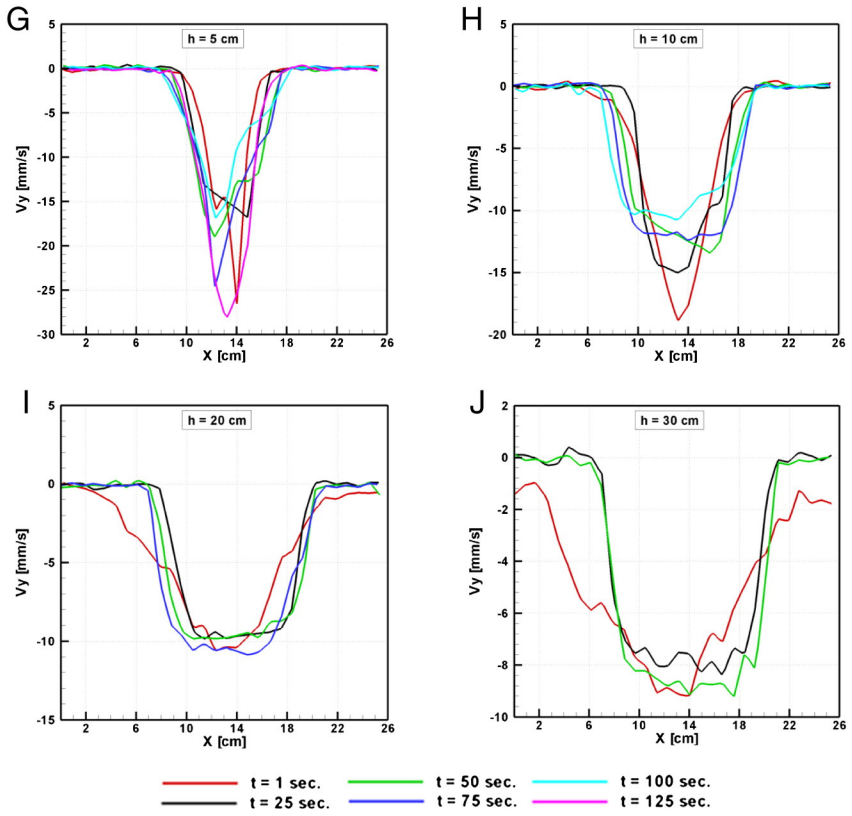


**Fig. 2** (*continued*).

Hartley's statistics $F_{max}$ and data given in Tables F, G, H, I and J in the Appendix:

$$F_{max} = \frac{S^2_{max}}{S^2_{min}}. \tag{6}$$

In this case for statistics $F_{max}$ from formula (6) the critical value with the significance level $\alpha = 0.05$ according to the distribution $F_{max}$ equals $F_{max\ critical} = F_{max;0.05;n-1;k}$, where $n$ denotes the number of repetitions of experiments for the given height $h$, $k$ denotes the number of comparisons of experimental readings for the given heights $h$.

In the case when the value of statistics calculated from formula (6) is higher than the critical value then the hypothesis of equality of variances can be rejected, in the other cases there is reason to reject the hypothesis of equality of variances.

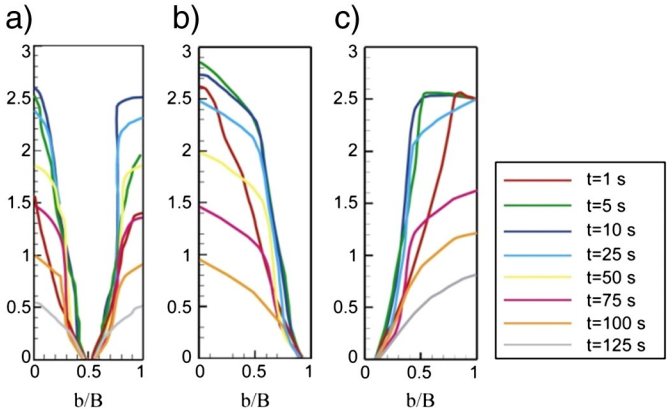


**Fig. 3.** Experimental measurements of the stagnant zone boundaries in the flowing flax seed in the case of eccentric filling and discharge: a) central, b) on the right, and c) on the left [34].

Calculations made according to formulas (4) and (5) are summarized in Table K given in the Appendix.

## 4. Empirical description of velocity $V_y$ of flowing grains in the model

We present two types of empirical descriptions of velocities of flowing grains in the silo model. The values of calculated coefficients of correlation confirm our choice of the function. If they are close to "1" or "−1" then empirical description is more precise.

### 4.1. Description by Gaussian bell curve

#### 4.1.1. Determining the constants in Gaussian bell curve by linearization

The proposed empirical function is of the following form:

$$V_y = A\, e^{Bx_1^2} \tag{7a}$$

where: $x_1 = |x - 13|$ cm, and $V_y = \frac{\overline{V}_{y,\ 13-n_i} + \overline{V}_{y,13+n_i}}{2}$.

When calculating the logarithm (7a) we obtain:

$$\ln V_y = \ln A + Bx_1^2. \tag{7b}$$

Denoting that

$$\ln V_y = Y, \quad \ln A = a, \quad x_1^2 = X_1 \tag{7c}$$

we obtain

$$Y = a + BX_1. \tag{7d}$$

From Eq. (7d) we determine parameters $a$ and $B$ using the method of the least squares and then the value $A = e^a$.

It is crucial to be convinced if the proposed formula (7a) is correct. To do this we can put experimental points on the functional scales.

Tracking the functional scale on horizontal ax $x_1^2$ and on the vertical ax $\ln V_y$ we can see that (Fig. 4a), the experimental points are put along the straight line. It can be proved for heights $h = 5, 10, 20, 30, 40$ [cm]. The coefficient of correlation confirms this for the straight line presented in formula (7d) and it is given in Table 1 as $|r|$.

The constants $A$ and $B$ were calculated by the least square method after linearization of formula (7a) and using data given in Tables A–E in the Appendix. Their values are listed in Table 1.

The constants $A$ and $B$ from Table 1 after the first regression depended on height $h = z$ according to formula (8) and are given in Table 1 in brackets.

$$A = 23.90 - 0.9124\,z + 0.01369\,z^2$$
$$B = -0.2239 + 0.0146\,z - 0.0002436\,z^2 \quad (8)$$

In this way using formulas (7a) and (8) we can calculate the flow velocity in any given point on demand position of this point and on the distance of the point from the axis of symmetry.

In Table 1 the absolute values of the coefficient of correlation $r$ for the straight line from formula (7d) and with velocity $V_y$ from formula (7a) are listed. The coefficients of correlation $R$ for all velocities $V_{y_i}$ are presented also in Table 1.

*4.1.2. The Gaussian description — nonlinear regression*

The constant values $A$ and $B$ from formula (7a) we can calculate by the Gauss–Newton method and with the nonlinear regression using the initial values of these constants from The constants $A$ and $B$ (given in Table 2) after the first regression depended on height $z = h$ according to formula (9) — a parabola of the second order.

$$A = 19.76 - 0.6187\,z + 0.00843\,z^2$$
$$B = -0.1635 + 0.01005\,z - 0.0001624\,z^2 \quad (9)$$

The values $A$ and $B$ after the second regression for level $z = h$ are given in Table 2 in brackets.

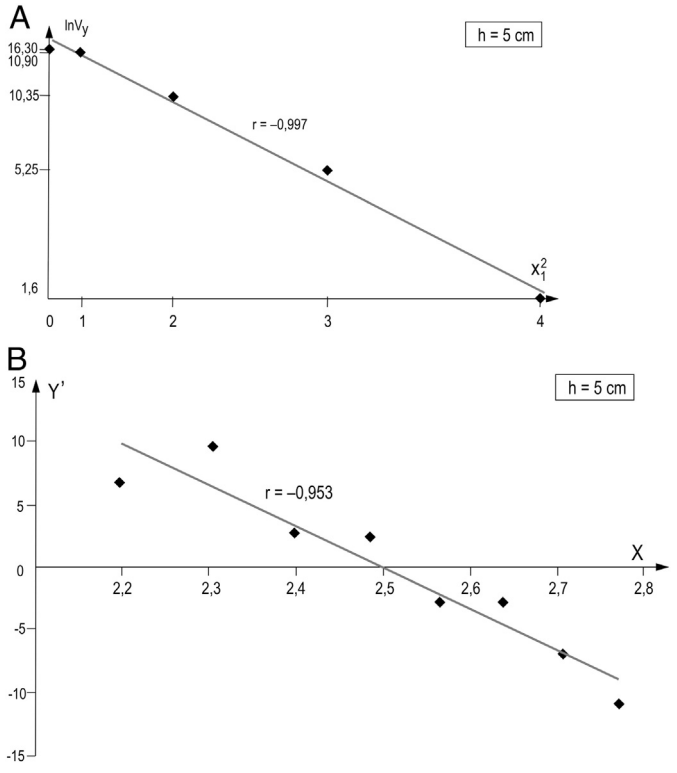


**Fig. 4.** A. Visualization of formula (7a) in the functional scales. B. Graphical form of derivatives from Eq. (10e) for $h = 5$ cm.

**Table 1**
The constant values $A$ and $B$ from formula (7a) after nonlinear regression.

| $h$ [cm] | 5 | 10 | 20 | 30 | 40 |
|---|---|---|---|---|---|
| Constant values | | | | | |
| $A$ | 20.10 (19.68) | 15.70 (16.14) | 10.59 (11.12) | 9.75 (8.85) | 8.95 (9.30) |
| $B$ | −0.1764 (−0.1569) | −0.075 (−0.102) | −0.0242 (−0.0288) | −0.0260 (−0.0431) | −0.0189 (−0.02857) |
| r | −0.992 | −0.989 | −0.969 | −0.962 | −0.935 |
| $R$ | 0.969 | 0.947 | 0.929 | 0.899 | 0.890 |

*4.2. Description of velocity $V_y$ of flowing grains by "the function of double logarithm"*

*4.2.1. Determining constants for the function of "double logarithm" by linearization*

The proposed empirical function for velocity is of the following form:

$$V_y = e^{A+B\ln x + C\ln^2 x}. \quad (10a)$$

Calculating the logarithm of Eq. (10a) we obtain:

$$\ln V_y = A + B\ln x + C\ln^2 x. \quad (10b)$$

Denoting that

$$\ln V_y = Y \text{ and } \ln x = X \quad (10c)$$

we obtain

$$Y = A + BX + CX^2. \quad (10d)$$

It is important to be convinced that if the description given in Eq. (10a) is made correctly we should verify if the description (10d) is correct. Eq. (10d) presents a parabola of the second order and the derivative $\frac{dY}{dX}$ presents the straight line. To check if the points which were calculated are put along the straight line we draw parabola through three successive points $i, j, k$, by using the Lagrange'a interpolating polynomial and then we calculate the following derivative:

$$\frac{dY}{dX}(X_j) = \frac{X_j - X_k}{(X_i - X_j)(X_i - X_k)}Y_i + \frac{2X_j - X_k - X_i}{(X_j - X_i)(X_j - X_k)}Y_j + \frac{X_j - X_i}{(X_k - X_i)(X_k - X_j)}Y_k. \quad (10e)$$

After calculating the derivative of Eq. (10e) we saw that the points are put close to the straight line (Fig. 4b).

We can present another graphical forms of Eq. (10e) for other levels $h = 10, 20, 30, 40$ cm. We can calculate the derivatives for these heights and create the straight lines.

The constant values $A$, $B$ and $C$ by linearization of formula (10a) were calculated by the least square method and are given in Table 3.

**Table 2**
The constant values $A$ and $B$ from formula (7a) after the nonlinear regression.

| $h$ [cm] | 5 | 10 | 20 | 30 | *40* |
|---|---|---|---|---|---|
| Constant values | | | | | |
| $A$ | 17.14 (16.88) | 14.06 (14.42) | 10.74 (10.76) | 9.04 (8.79) | 8.39 (8.50) |
| $B$ | −0.132 (−0.117) | −0.0573 (−0.0791) | −0.0280 (−0.0272) | −0.0200 (−0.0078) | −0.015 (−0.021) |
| $R$ | 0.992 | 0.965 | 0.934 | 0.919 | 0.941 |

**Table 3**
The constant values from formula (10a) calculated by using the linear regression.

| $h$ [cm] | 5 | 10 | 20 | 30 | 40 |
|---|---|---|---|---|---|
| Constant values | | | | | |
| $A$ | −136.37 (−141.84) | −81.53 (−70.36) | −41.84 (−34.61) | −15.47 (−22.70) | −11.05 (−16.74) |
| $B$ | 109.71 (114.29) | 67.34 (57.90) | 35.38 (29.71) | 14.41 (20.31) | 10.97 (15.61) |
| $C$ | −21.62 (−22.55) | −13.44 (−11.49) | −7.05 (−5.96) | −2.94 (−4.12) | −2.28 (−3.20) |
| $R$ | 0.983 | 0.873 | 0.805 | 0.920 | 0.889 |

The constant values $A$, $B$ and $C$ given in Table 3 depended on height $z = h$ according to formula (11):

$$A = 1.130 - 714.88\,\frac{1}{z},\quad r = -0.987$$
$$B = 1.513 + 563.86\,\frac{1}{z},\quad r = 0.985 \qquad (11)$$
$$C = -0.434 - 110.60\,\frac{1}{z},\quad r = -0.985.$$

The values calculated from formula (11) are given in Table 3 in brackets.

*4.2.2. Description of velocity $V_y$ using the nonlinear regression*

The constant values $A$, $B$ and $C$ from formula (10a) we can calculate by the Levenberg–Marquardt method and with the nonlinear regression using the initial values of these constants given in Table 3. Their values after the nonlinear regression are presented in Table 4.

The constant values $A$, $B$ and $C$ given in Table 4 depended on height $z = h$ according to formula (12).

$$A = 10.696 - 756.66\,\frac{1}{z},\quad r = -0.998$$
$$B = -5.906 + 593.51\,\frac{1}{z},\quad r = 0.998 \qquad (12)$$
$$C = 1.089 - 115.77\,\frac{1}{z},\quad r = -0.988.$$

The values of these parameters calculated for $z = h$ after the second regression are listed in Table 4 in brackets.

## 5. Analysis of empirical results

*5.1. Comparison of empirical description with experimental results*

In Figs. 5, 7, 9, 11, and 13 the comparison of experimental results with empirical description by the function of Gaussian type according to formula (7a) and using data given in Tables 1 and 2 is presented.

In Figs. 6, 8, 10, 12, and 14 the results of empirical description by function of "the double logarithm" according formula (10a) using the data from Tables 3 and 4 are presented.

In Figs. 5–14 the constant values for the empirical description were determined by the method of linearization (linear regression is denoted as solid lines) and by the method of nonlinear regression (dotted lines).

**Table 4**
Constant values for formula (10a) calculated by using the nonlinear regression.

| $h$ [cm] | 5 | 10 | 20 | 30 | 40 |
|---|---|---|---|---|---|
| Constant values | | | | | |
| $A$ | −143.62 (−141.24) | −59.46 (−65.67) | −28.76 (−27.74) | −16.98 (−15.23) | −9.67 (−8.82) |
| $B$ | 114.63 (112.80) | 48.74 (53.45) | 24.59 (23.76) | 15.25 (13.88) | 9.61 (8.93) |
| $C$ | −22.43 (−22.07) | −9.56 (−10.49) | −4.85 (−4.70) | −3.03 (−2.77) | −1.96 (−1.81) |
| $R$ | 0.994 | 0.968 | 0.918 | 0.928 | 0.920 |

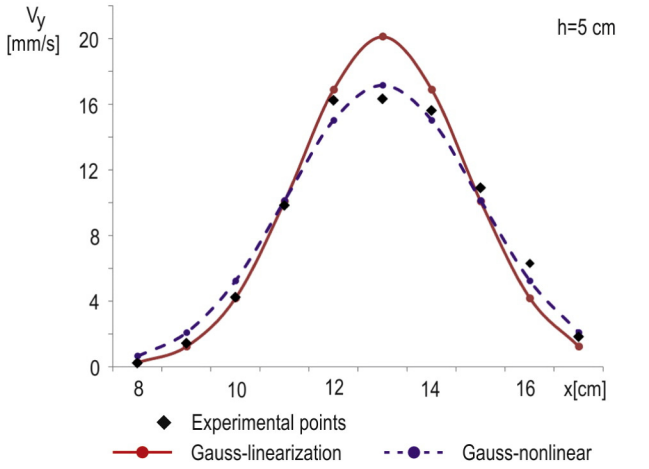


**Fig. 5.** Experimental results of velocities $V_y$ and their empirical descriptions on level $h = 5$ cm.

In these figures we can see a good agreement of both descriptions but the better compatibility to the experimental results was obtained by using the nonlinear regression. In Figs. 5, 7, 9, 11, and 13 the comparison between experimental results and the empirical description (Gaussian function) according to formula (7a) with data given in Tables 1 and 2 is presented. In Figs. 4, 6, 8, 10, and 12 the comparison between the experimental results and the empirical description ("the double logarithm" function) according to formula (10a) with using data given in Tables 3 and 4 is presented.

Analyzing Figs. 5–14 we can notice differences in empirical descriptions when determining the constant values in functions calculated by the method of linearization (formulas 7a or 10a) and also in the case of using the nonlinear regression. The better description was obtained using the nonlinear regression (the dotted lines in Figs. 5–14). When comparing the results, we can see that a special large discrepancy in empirical descriptions occurred in description for lower levels ($h = 5$, 10, 20 cm). There are also differences both in the Gaussian description and in the function of "the double logarithm". In the first case we obtained symmetrical description relative to the symmetry axis of silo model, i.e. to the location of points at $x = 13$ cm, in the other cases, the description is not symmetrical due to the shape of the empirical function. These conclusions are also supported by the sum of the squares of differences $\sum\left(V_{y_{i\ exp}} - V_{y_{i\ emp}}\right)^2$ that is presented in Table 5a.

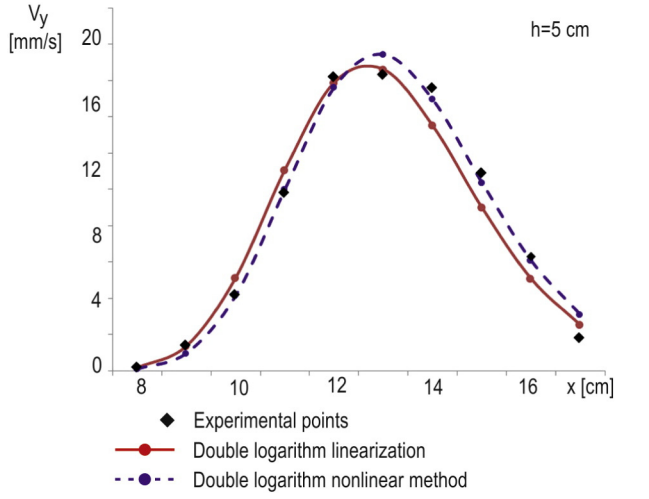


**Fig. 6.** Experimental results of velocities $V_y$ and their empirical descriptions on level $h = 5$ cm.

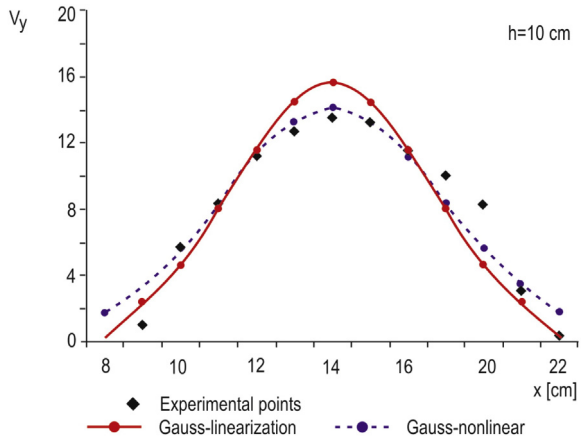


**Fig. 7.** Experimental results of velocities $V_y$ and their empirical descriptions on level $h = 10$ cm.

Now we will present the comparative analysis of the coefficients of correlation and also corrected coefficients of correlation. Regular multiple correlation coefficients $R$ are calculated from the following formula:

$$R = \sqrt{1 - \frac{\sum_{1}^{n}\left(V_{y_i} - \hat{V}_{y_i}\right)^2}{\sum_{1}^{n}\left(V_{y_i} - \overline{V}_y\right)^2}} \qquad \text{(R1)}$$

where: $V_{y_i}$ — measured experimental velocity, $\hat{V}_{y_i}$ — velocity calculated from regression, $\overline{V}_y$ — average experimental velocity, $n$ — number of experimental points for given height $h$.

Values of $R$ were calculated from formula (R1) and given in Tables 1, 2, 3 and 4, respectively.

Corrected correlation coefficient $R_s$ was calculated from the following formula:

$$R_s = \sqrt{1 - \frac{\sum_{1}^{n}\left(V_{y_i} - \hat{V}_{y_i}\right)^2/(n-K)}{\sum_{1}^{n}\left(V_{y_i} - \overline{V}_y\right)^2/(n-1)}} \qquad \text{(R2)}$$

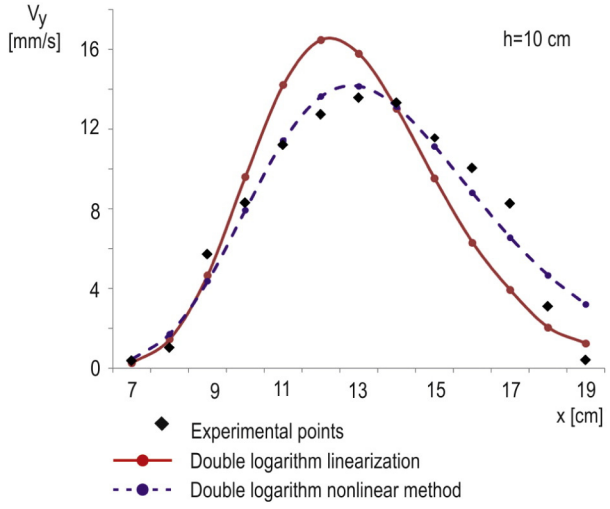


**Fig. 8.** Experimental results of velocities $V_y$ and their empirical descriptions on level $h = 10$ cm.

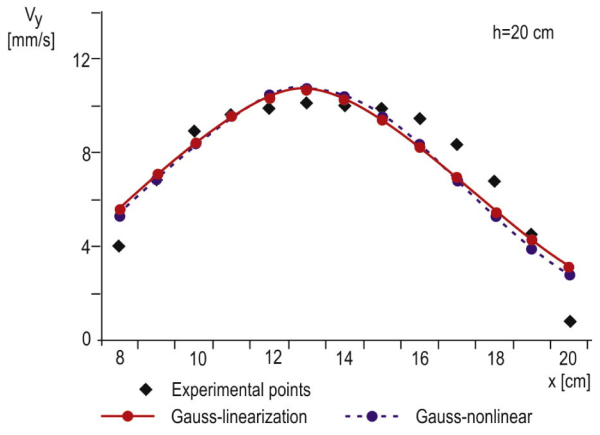


**Fig. 9.** Experimental results of velocities $V_y$ and their empirical descriptions on level $h = 20$ cm.

where: $K$ — number of constants in the regression equation and $K = 2$ for the Gaussian method and $K = 3$ for the method of "double logarithm".

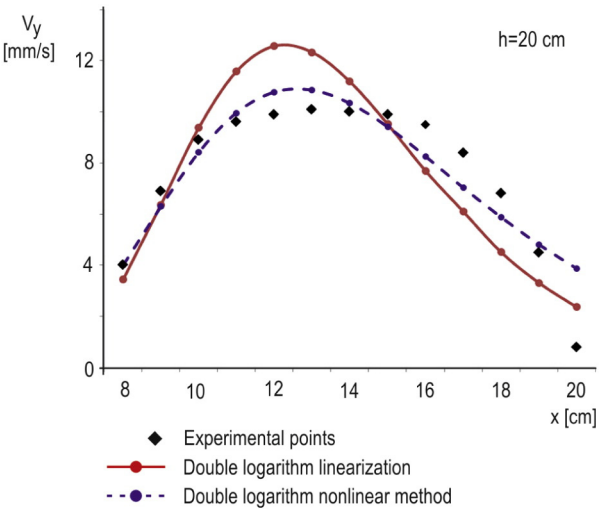


**Fig. 10.** Experimental results of velocities $V_y$ and their empirical descriptions on level $h = 20$ cm.

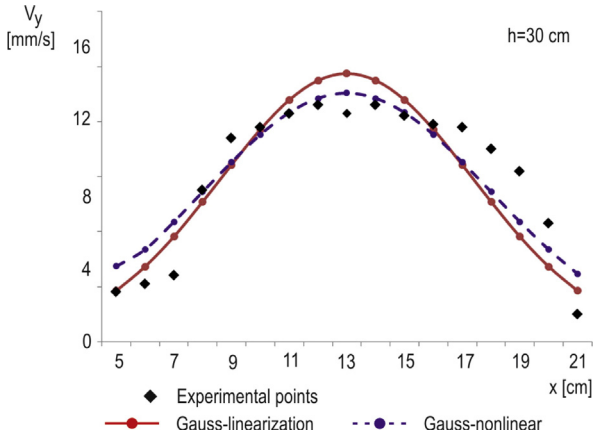


**Fig. 11.** Experimental results of velocities $V_y$ and their empirical descriptions on level $h = 30$ cm.

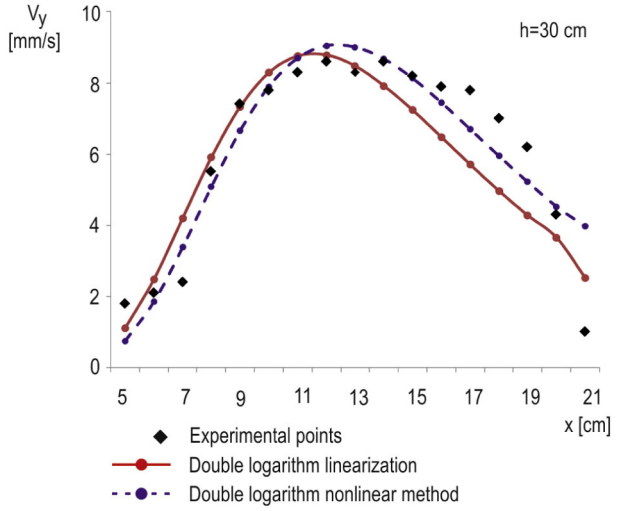


**Fig. 12.** Experimental results of velocities $V_y$ and their empirical descriptions on level $h = 30$ cm.

In Table 5b the coefficient of correlation $R$ and corrected coefficients $R_s$ are listed.

When analyzing the data given in Table 5b we can notice rather small differences between the regular multiple correlation coefficients and the corrected ones for the Gaussian method with the number of regression constants $K = 2$. A little higher differences between these coefficients can be noticed for the method of "double logarithm" with the number of constants $K = 3$ especially for linearization.

*5.2. Predicting velocities due to extrapolation*

*5.2.1. Predicting velocities due to the nonlinear Gaussian description*

Using formula (9) for level $h = 50$ cm we obtain values of parameters $A$ and $B$ as follows:

$$A(h = 50\,\text{cm}) = 9.9 \;\text{ and }\; B(h = 50\,\text{cm}) = -0.07. \tag{13}$$

Substituting formula (13) to formula (7a) we obtain the predicted values of velocities:

$$V_y = 9.9\, e^{-0.07x_1^2}. \tag{14}$$

The calculations according to formula (14) and the experimental results are given in Table 6.

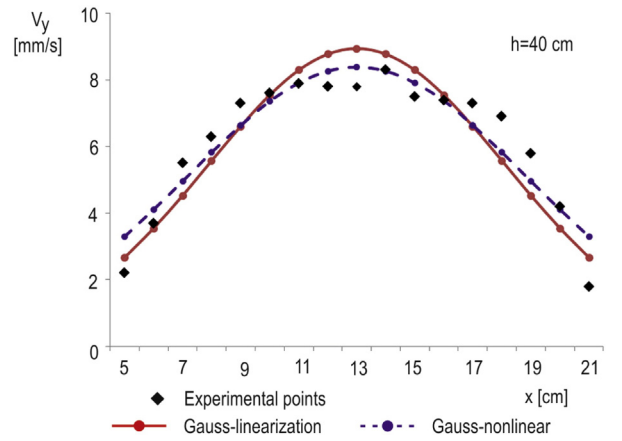


**Fig. 13.** Experimental results of velocities $V_y$ and their empirical descriptions on level $h = 40$ cm.

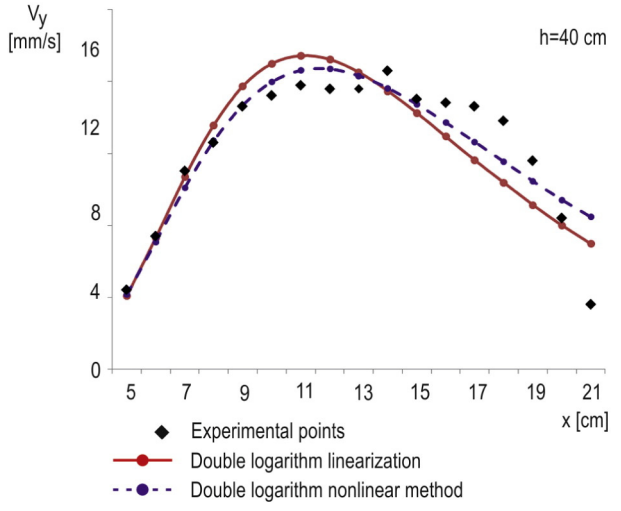


**Fig. 14.** Experimental results of velocities $V_y$ and their empirical descriptions on level $h = 40$ cm.

*5.2.2. Predicting velocities $V_y$ due to the nonlinear description of "the double logarithm" function*

Using formula (12) we calculate the constant values $A$, $B$ and $C$ for level $z = 50$ cm

$$A(50\,\text{cm}) = -5.037, B(50\,\text{cm}) = 5.964, C(50\,\text{cm}) = -1.23. \tag{15}$$

Substituting the calculated values from formula (15) to formula (10a) we obtain formula to calculate velocities as follows:

$$V_y = e^{-5.037+5.964\ln x-1.23\ln^2 x}. \tag{16}$$

The calculated values of velocities according formula (16) are listed in Table 7. For comparison and for more clear understanding

**Table 5a**
Comparison of the sums of the squares of differences of velocities for points located at 8 cm ≤ $x$ ≤ 17 cm.

| $h$ [cm] | $\sum\left(V_{y_{i\ exp}} - V_{y_{i\ emp}}\right)^2$ | | | |
|---|---|---|---|---|
| | Gaussian method | | Method of double logarithm | |
| | Linearization | Nonlinear method of Gauss–Newton | Linearization | Nonlinear method of Levenberg–Marquardt |
| 5 | 22.02 | 6.09 | 12.62 | 4.31 |
| 10 | 30.56 | 16.85 | 70.22 | 9.13 |
| 20 | 7.15 | 6.87 | 32.23 | 5.35 |
| 30 | 9.75 | 3.27 | 8.46 | 2.57 |
| 40 | 4.86 | 2.16 | 6.36 | 2.26 |

**Table 5b**
Comparative summary of correlation coefficients $R$ and corrected correlation coefficients $s$ $R_S$.

| Method of description | | $h$ [cm] | | | | |
|---|---|---|---|---|---|---|
| | | 5 | 10 | 20 | 30 | 40 |
| "Gauss" linearization | $R$ | 0.969 | 0.947 | 0.929 | 0.899 | 0.890 |
| | $R_s$ | 0.965 | 0.942 | 0.922 | 0.892 | 0.889 |
| "Gauss" nonlinear | $R$ | 0.995 | 0.965 | 0.934 | 0.919 | 0.941 |
| | $R_s$ | 0.991 | 0.962 | 0.928 | 0.914 | 0.937 |
| "Double logarithm" linearization | $R$ | 0.983 | 0.873 | 0.805 | 0.920 | 0.889 |
| | $R_s$ | 0.978 | 0.846 | 0.760 | 0.884 | 0.873 |
| "Double logarithm" nonlinear | $R$ | 0.994 | 0.968 | 0.918 | 0.928 | 0.920 |
| | $R_s$ | 0.992 | 0.961 | 0.900 | 0.917 | 0.908 |

**Table 6**
The results of predicted and experimental velocities $V_y$ for level $h = 50$ cm due to the Gaussian method.

| $x$ [cm] | 6 | 7 | 8 | 9 | 10 | 11 | 12 | 13 | 14 | 15 | 16 | 17 | 18 | 19 | 20 |
|---|---|---|---|---|---|---|---|---|---|---|---|---|---|---|---|
| $V_y$ [mm/s] | | | | | | | | | | | | | | | |
| $V_{y\ predicted}$ | 0.32 | 0.8 | 1.72 | 3.23 | 5.27 | 7.48 | 9.23 | 9.9 | 9.23 | 7.48 | 5.27 | 3.23 | 1.72 | 0.8 | 0.32 |
| $\overline{V}_{y\ exp}$ | 6.4 | 6.6 | 7.1 | 7.5 | 7.5 | 7.5 | 7.6 | 7.6 | 7.6 | 6.6 | 7.4 | 6.6 | 6.3 | 5.8 | 3.5 |

**Table 7**
Results of the predicted values of velocities for level $h = 50$ cm were calculated due to the method of "the double logarithm".

| $x$ [cm] | 6 | 7 | 8 | 9 | 10 | 11 | 12 | 13 | 14 | 15 | 16 | 17 | 18 | 19 | 20 |
|---|---|---|---|---|---|---|---|---|---|---|---|---|---|---|---|
| $V_y$ [mm/s] | | | | | | | | | | | | | | | |
| $V_{y\ predicted}$ | 5.47 | 6.76 | 7.74 | 8.41 | 8.80 | 8.95 | 8.92 | 8.74 | 8.46 | 8.11 | 7.72 | 7.29 | 6.86 | 6.42 | 6.0 |
| $\overline{V}_{y\ exp}$ | 6.4 | 6.6 | 7.1 | 7.5 | 7.5 | 7.5 | 7.6 | 7.6 | 7.6 | 6.6 | 7.4 | 6.6 | 6.3 | 5.8 | 3.5 |

of the analysis, the values $\overline{V}_{y\ exp}$ which were calculated in Table 6, are repeated in Table 7.

### 5.3. Prediction velocities of flowing grains by using interpolation

#### 5.3.1. Prediction velocities due to the nonlinear model of the Gaussian type

Using formula (9) we also calculate the constant values $A$ and $B$ for level $z = 15$ cm and their values are following:

$$A(15\,\text{cm}) = 14.82, B(15\,\text{cm}) = -0.0442. \tag{17}$$

Substituting the parameters from formula (17) to formula (7a) we obtain expression for velocity, from which we can calculate velocities for corresponding values, $x_1$:

$$V_y = 14.82\, e^{-0.0442x_1^2}. \tag{18}$$

Detailed calculations of velocities due to formula (18) are given in Table 8, where we also put the experimental results for more clear comparison and analysis.

#### 5.3.2. Prediction velocities due to the nonlinear function of "the double logarithm"

Using formula (12) for level $z = 15$ cm we obtain values of constant parameters as follows:

$$A(15\,\text{cm}) = -40.35, B(15\,\text{cm}) = 33.66, C(15\,\text{cm}) = -6.63. \tag{19}$$

Substituting values from formula (19) to formula (10a), we obtain the expression for velocities:

$$V_y = e^{-40.35+33.66\ln x-6.63\ln^2 x}. \tag{20}$$

**Table 8**
Results for interpolation obtained for level $h = 15$ cm due to the Gaussian method.

| $x$ [cm] | 6 | 7 | 8 | 9 | 10 | 11 | 12 | 13 | 14 | 15 | 16 | 17 | 18 | 19 | 20 |
|---|---|---|---|---|---|---|---|---|---|---|---|---|---|---|---|
| $V_y$ [mm/s] | | | | | | | | | | | | | | | |
| $V_{y\ interpol}$ | 1.7 | 3.02 | 4.91 | 7.31 | 9.96 | 12.42 | 14.18 | 14.82 | 14.18 | 12.42 | 9.96 | 7.31 | 4.91 | 3.02 | 1.7 |
| $\overline{V}_{y\ exp}$ | 0 | 0.4 | 5.5 | 8.6 | 10.1 | 10.6 | 10.5 | 10.5 | 10.5 | 9.4 | 9.9 | 8.6 | 5.5 | 4 | 0.25 |

**Table 9**
The results of predicted velocities by using interpolation for level $h = 15$ cm according to the method of "the double logarithm."

| $x$ [cm] | 6 | 7 | 8 | 9 | 10 | 11 | 12 | 13 | 14 | 15 | 16 | 17 | 18 | 19 | 20 |
|---|---|---|---|---|---|---|---|---|---|---|---|---|---|---|---|
| $V_y$ [mm/s] | | | | | | | | | | | | | | | |
| $V_{y\ interpol}$ | 0.29 | 1.17 | 3.02 | 5.73 | 8.69 | 11.18 | 12.66 | 13.0 | 12.36 | 11.04 | 9.39 | 7.67 | 6.06 | 4.66 | 3.51 |
| $\overline{V}_{y\ exp}$ | 0 | 0.4 | 5.5 | 8.6 | 10.1 | 10.6 | 10.5 | 10.5 | 10.5 | 9.4 | 9.9 | 8.6 | 5.5 | 4.0 | 0.25 |

**Table 10**
Values of the flow rate.

| $h$ [cm] | $x_{min}$ | $x_{max}$ | Flow rate Q [cm$^2$/s] | | | |
|---|---|---|---|---|---|---|
| | | | Gaussian method | | Method of "the double logarithm" | |
| | | | Nonlinear regression | Nonlinear regression according to formula (23) and constants from Table 11 | Nonlinear regression | Nonlinear regression according to formula (23) and constants from Table 11 |
| 5 | 8 | 17 | 8.15 | 8.17 | 7.74 | 7.75 |
| 10 | 6 | 20 | 10.23 | 10.08 | 10.34 | 10.27 |
| 20 | 7 | 21 | 10.16 | 10.47 | 10.48 | 10.59 |
| 30 | 4 | 22 | 10.52 | 10.52 | 10.50 | 10.56 |
| 40 | 4 | 22 | 10.70 | 10.53 | 10.63 | 10.52 |

**Table 11**
The results obtained from formulas (23) to (24).

| Method of description | *a* | *b* | *c* | *R* |
|---|---|---|---|---|
| Gaussian — linearization | 10.315 | 4.581 | −69.278 | 0.9766 |
| Gaussian — nonlinear | 10.489 | 3.320 | −74.533 | 0.9652 |
| "Double logarithm" — linearization | 10.069 | 10.275 | −108.019 | 0.9963 |
| "Double logarithm" — nonlinear | 10.283 | 12.467 | −125.66 | 0.9973 |

The calculations according to formula (20) are listed in Table 9, where we also put the experimental values which were given in Table 8.

## 6. Analysis of flow rate in the model

Using the values given in Tables A–E presented in the Appendix, we determined points where velocity $V_y = 0$ and the coordinates of these points ($x_{min}$, $x_{max}$, respectively) are presented in Table 10. Then we use formula (7a) to determine flow rate due to description of velocities by the method of the Gaussian function.

$$Q = \int_{x_{min}}^{13} Ae^{Bx^2}\,dx + \int_{13}^{x_{max}} Ae^{Bx^2}\,dx \tag{21}$$

where constant values *A* and *B* are presented in Table 2 (using the nonlinear regression).

Calculating the flow rate when describing velocities by the method of "the double logarithm" we use the following formula:

$$Q = \int_{x_{min}}^{x_{max}} e^{A+B\ln x + C\ln^2 x}\,dx \tag{22}$$

where the constant values *A*, *B* and *C* were taken from Table 4 using the nonlinear regression. The calculations are listed in Table 10.

The flow rate *Q* presented in Table 10 was described by the following function:

$$\hat{Q} = a + \frac{b}{h} + \frac{c}{h^2}. \tag{23}$$

The constant values *A*, *B*, and *C* were determined by the method of the least squares and their values are presented in Table 11, where the coefficient of correlation *R* is also given and it was calculated according to the formula:

$$R = \sqrt{1 - \frac{\sum\left(Q_i - \hat{Q}_i\right)^2}{\sum\left(Q_i - \overline{Q}\right)^2}} \tag{24}$$

where $Q_i$ denotes the flow rate calculated according to formula (21), $\hat{Q}_i$ denotes the flow rate for various heights *h* calculated according formula (23), and $\overline{Q}$ denotes the average values of the flow rate.

The results of the values of flow rate calculated according to formula (23) with the constant values taken from Table 11 are presented in Table 10.

On the base of data given in Table 10, the values of flow rate calculated according to formula (23) are presented in Figs. 15–16. In these figures the points present the flow rate calculated according to formulas (21–22) and values *Q* are given in Table 10. The solid lines present the regression curves according formula (23) and the values *Q* are given in Table 10.

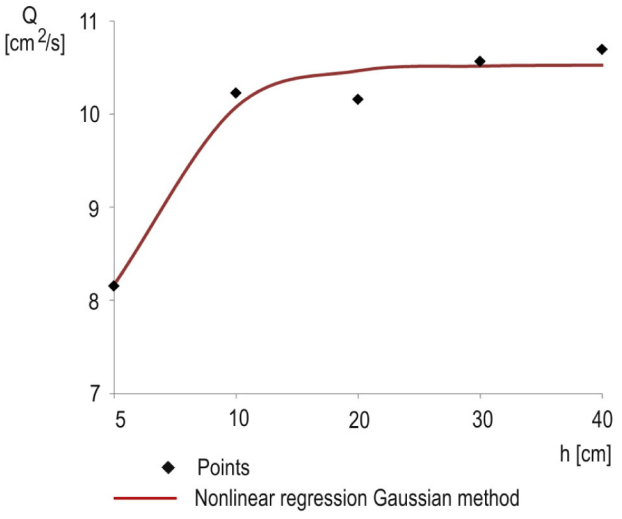


**Fig. 15.** Values of the flow rate calculated according to formula (23) for empirical description by applying the function of the Gaussian type — nonlinear.

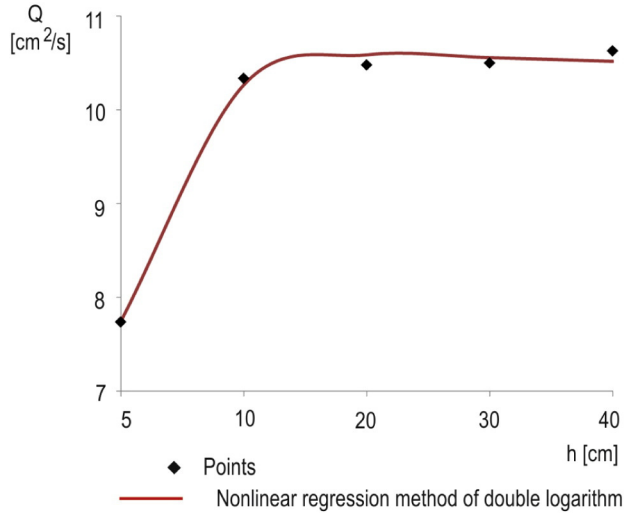


**Fig. 16.** Values of the flow rate calculated according to formula (23) for empirical description by applying the function type of "the double logarithm" — nonlinear.

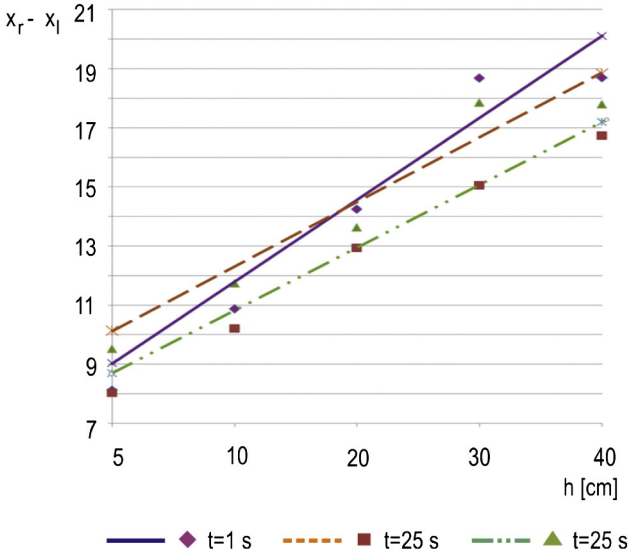


**Fig. 17.** Range of the stagnant boundary at the analyzed instants of the flow.

## 7. Empirical description of stagnant zones boundaries

In Table L given in the Appendix a certain set of data is determined. They are $x_1$ and $x_2$, where $x_1$ is the distance from the left side of the model where velocity $V_y$ is equal to zero and $x_2$ is the distance from the right side of the model, where $V_y$ is also equal to zero. These distances were appointed for time instants $t = 1, 25, 50$ s and for levels $h = 5, 10, 20, 30, 40$ cm.

On the base of values of $x_1$ and $x_2$ the difference $x = x_2 - x_1$ was calculated where $V_y \neq 0$. This difference was described by the linear function:

$$\begin{aligned} &t = 1\ [s], \quad \hat{x} = x_2 - x_1 = 7.45 + 0.3166\,h, \quad r = 0.965 \\ &t = 25\ [s], \quad \hat{x} = x_2 - x_1 = 7.47 + 0.2433\,h, \quad r = 0.988 \\ &t = 50\ [s], \quad \hat{x} = x_2 - x_1 = 8.88 + 0.2485\,h, \quad r = 0.964. \end{aligned} \tag{25}$$

Critical values $r_k = 0.878$ for significance level $\alpha = 0.05$ and for $5 - 2 = 3$ degrees of freedom according to publication [45].

In Fig. 17 the relations (25) are presented in the graphical form.

## 8. Conclusions

We can draw out a few significant conclusions and discuss them. They are the following:

1. Rejection "the thick" statistical errors calculated according to formulas (1) and (2), which are given in Tables A, B, C, D, and E in the Appendix, and comparing with the critical value $K_{crit}$ leads to the conclusion that it occurs rather seldom for locations of extreme points where velocities are close to zero.
2. Comparing data given in Tables A–E with data in Tables F–J given in the Appendix, where the calculations of confidence interval for significant levels $\alpha = 0.05$ are presented, we see that time does not have influence to velocities.
3. Description of velocities of flow by the function of the Gaussian type, i.e. formula (7a) and the function of "the double logarithm", i.e. formula (10a), is presented in this paper. The constant values to these formulas were calculated by two methods, by the linearization of these functions or by using the nonlinear regression. Figs. 5–14 confirm that much better description, when calculating the constant values, was obtained when using nonlinear regression. Also data given in Table 5a where the sum of squares of the differences of velocities (using the nonlinear regression), is even a few times lower than using the linearization. Analyzing data in Table 5a we see that the better description can be obtained by using the function of "the double logarithm".
4. The above conclusion is further confirmed by comparison of Table 6 with Table 7 and Table 8 with Table 9, respectively. Analyzing data in Tables 6 and 7 we see that using extrapolation it makes it possible to obtain results of velocities much more close to the experimental values when using the function of "the double logarithm". The same conclusion can be drawn when analyzing data obtained by interpolation and presented in Tables 8 and 9. Especially this conclusion is true for the points located further from the symmetry axis of the silo.
5. Analyzing the curves presented in Figs. 15–16 we can see that the flow rate has different values in the volume up to $h = 10$ cm. Higher than this level the flow rate is stabilized.
6. In Fig. 17 we analyzed the stagnant zone boundaries. They were linear as presented between level $h = 5$ and up to $h = 40$ cm. This fact was also proved by formula (25) where we see the high value of the Pearson coefficient of correlation and it is higher than the critical value for the significant level $\alpha = 0.05$.

## Acknowledgments

The experiments were performed in the Institute of Fundamental Technological Research Polish Academy of Sciences using the equipment and software for DPIV technique. Statistical analysis was done using the software Statistica10.

## Appendix

Statistical analysis of experimental results.

**Table A**
Readings at level $h = 5$ cm.

| Time $t$ [s] | $V_y$ [mm/s] for the distance from the left wall $x$ [cm] | | | | | | | | | |
|---|---|---|---|---|---|---|---|---|---|---|
| | 8 | 9 | 10 | 11 | 12 | 13 | 14 | 15 | 16 | 17 |
| 1 | 0.25 | 0.5 | 1 | 6 | 15 | 14.5 | 26 | 7 | 1 | 0.5 |
| 25 | 0 | 0 | 2 | 10 | 14 | 15 | 16 | 17 | 6 | 0.5 |
| 50 | 0 | 0.5 | 6 | 12 | 18 | 17 | 13 | 12.5 | 11 | 2.5 |
| 75 | 0.25 | 3 | 6 | 11 | 19 | 20 | 14 | 11 | 8 | 2 |
| 100 | 0.5 | 3 | 6 | 10 | 15 | 15 | 9 | 7 | 5.5 | 3.5 |
| $K$ | 1.009 | 1.213 | 1.437 | 1.862 | 1.444 | 1.814 | 1.832 | 1.628 | 1.616 | 1.316 |

$\alpha = 0.05$, $K_{kr} = 1.869$.

**Table B**
Readings at level $h = 10$ cm.

| Time $t$ [s] | $V_y$ [mm/s] for the distance from the left wall $x$ [cm] | | | | | | | | | | | | | | |
|---|---|---|---|---|---|---|---|---|---|---|---|---|---|---|---|
| | 7 | 8 | | 9 | 10 | 11 | 12 | 13 | 14 | 15 | 16 | 17 | | 18 | 19 |
| | | Before rejecting | After rejecting | | | | | | | | | Before rejecting | After rejecting | | |
| 1 | 1 | 1 | 1 | 3 | 6 | 10 | 15 | 18 | 17.5 | 13 | 8 | 3.5 | – | 1 | 0 |
| 25 | 0 | 0 | 0 | 0.5 | 4 | 13 | 14.5 | 15 | 14.5 | 11 | 10 | 6 | 6 | 0.5 | 0 |
| 50 | 0 | 1 | 1 | 6 | 10 | 11 | 11.5 | 12 | 12.5 | 13 | 13 | 9 | 9 | 3 | 0.5 |
| 75 | 0.25 | 2 | 2 | 9 | 11.5 | 12 | 12 | 12 | 12.5 | 12 | 12 | 10.5 | 10.5 | 6 | 1 |
| 100 | 0.5 | 6 | – | 10 | 10 | 10 | 10.5 | 10.75 | 9.75 | 8.75 | 8.5 | 7.5 | 7.5 | 5 | 0.5 |
| $K$ | 0.936 | 1.907 | 1.414 | 1.455 | 1.524 | 1.544 | 1.315 | 1.693 | 1.563 | 1.768 | 1.392 | 2.354 | 1.341 | 1.346 | 1.604 |

$\alpha = 0.05$, $K_{kr} = 1.869$.

**Table C**
Readings at level $h = 20$ cm.

| Time $t$ [s] | $V_y$ [mm/s] for the distance from the left wall $x$ [cm] | | | | | | | | | | | | | | | | |
|---|---|---|---|---|---|---|---|---|---|---|---|---|---|---|---|---|---|
| | 3 | | 4 | | 5 | | 6 | | 7 | | 8 | 9 | 10 | 11 | 12 | 13 | 14 |
| | Before rejecting | After rejecting | Before rejecting | After rejecting | Before rejecting | After rejecting | Before rejecting | After rejecting | Before rejecting | After rejecting | | | | | | | |
| 1 | 0.5 | 0 | 1 | 0 | 2 | 0 | 3 | 0 | 4 | 0 | 5 | 5.5 | 8 | 9 | 10 | 10.25 | 10 |
| 25 | 0 | 0 | 0 | 0 | 0 | 0 | 0 | 0 | 0 | 0 | 1 | 5 | 8 | 9.5 | 9.5 | 9.75 | 9.75 |
| 50 | 0 | 0 | 0 | 0 | 0 | 0 | 0 | 0 | 0 | 0 | 3 | 8 | 9.5 | 9.75 | 9.75 | 9.75 | 9.75 |
| 75 | 0 | 0 | 0 | 0 | 0 | 0 | 0 | 0 | 0 | 0 | 7 | 9 | 10 | 10.25 | 10.5 | 10.5 | 10.5 |
| $K$ | 1.728 | 0 | 1.732 | 0 | 1.732 | 0 | 2.261 | 0 | 1.732 | 0 | 1.341 | 1.195 | 1.254 | 1.397 | 1.509 | 1.354 | 1.633 |

$\alpha = 0.05$, $K_{kr} = 1.689$.

**Table C** (*continued*)
Readings at level $h = 20$ cm.

| Time $t$ [s] | $V_y$ [mm/s] for the distance from the left wall $x$ [cm] | | | | | | | | | | | | | | | | | |
|---|---|---|---|---|---|---|---|---|---|---|---|---|---|---|---|---|---|---|
| | 15 | 16 | 17 | 18 | 19 | 20 | 21 | | 22 | | 23 | | 24 | | 25 | | 26 | |
| | | | | | | | Before rejecting | After rejecting | Before rejecting | After rejecting | Before rejecting | After rejecting | Before rejecting | After rejecting | Before rejecting | After rejecting | Before rejecting | After rejecting |
| 1 | 9.75 | 8.5 | 6.5 | 4.5 | 3 | 1.75 | 1 | 0 | 1 | 0 | 0.75 | 0 | 0.75 | 0 | 0.75 | 0 | 0.75 | 0 |
| 25 | 9.5 | .5 | 9.5 | 8.25 | 4 | 0 | 0 | 0 | 0 | 0 | 0 | 0 | 0 | 0 | 0 | 0 | 0 | 0 |
| 50 | 9.5 | 9.5 | 8.75 | 8.5 | 6 | 0.25 | 0 | 0 | 0 | 0 | 0 | 0 | 0 | 0 | 0 | 0 | 0 | 0 |
| 75 | 10.75 | 10.5 | 9 | 6 | 5 | 1 | 0 | 0 | 0 | 0 | 0 | 0 | 0 | 0 | 0 | 0 | 0 | 0 |
| $K$ | 1.689 | 1.414 | 1.651 | 1.398 | 1.271 | 1.460 | 1.732 | 0 | 1.732 | 0 | 1.723 | 0 | 1.724 | 0 | 1.723 | 0 | 1.723 | 0 |

**Table D**
Readings at level $h = 30$ cm.

| Time $t$ [s] | $V_y$ [mm/s] for the distance from the left wall $x$ [cm] | | | | | | | | | | | | | | | | | | |
|---|---|---|---|---|---|---|---|---|---|---|---|---|---|---|---|---|---|---|---|
| | 0 | | 1 | | 2 | | 3 | | 4 | | 5 | 6 | 7 | 8 | 9 | 10 | 11 | 12 | 13 |
| | Before rejecting | After rejecting | Before rejecting | After rejecting | Before rejecting | After rejecting | Before rejecting | After rejecting | Before rejecting | After rejecting | | | | | | | | | |
| 1 | 1 | 0 | 1 | 0 | 1 | 0 | 2 | 0 | 4 | 0 | 5 | 5.75 | 5.75 | 6 | 7 | 7.75 | 9 | 9 | 9 |
| 25 | 0 | 0 | 0 | 0 | 0 | 0 | 0 | 0 | 0 | 0 | 0 | 0 | 0.5 | 5.5 | 7.25 | 7.5 | 7.5 | 8 | 7.5 |
| 50 | 0 | 0 | 0 | 0 | 0 | 0 | 0 | 0 | 0 | 0 | 0.5 | 0.5 | 1 | 5 | 8 | 8.25 | 8.25 | 8.75 | 8.5 |
| $K$ | 1.422 | 0 | 1.422 | 0 | 1.414 | 0 | 1.415 | 0 | 1.416 | 0 | 1.410 | 1.412 | 1.407 | 1.225 | 1.365 | 1.365 | 1.226 | 1.365 | 1.330 |

$\alpha = 0.05$, $K_{kr} = 1.412$.

**Table D** (*continued*)
Readings at level $h = 30$ cm.

| Time $t$ [s] | $V_y$ [mm/s] for the distance from the left wall $x$ [cm] | | | | | | | | | | | | | | | | | |
|---|---|---|---|---|---|---|---|---|---|---|---|---|---|---|---|---|---|---|
| | 14 | 15 | 16 | 17 | 18 | 19 | 20 | 21 | 22 | | 23 | | 24 | | 25 | | 26 | |
| | | | | | | | | | Before rejecting | After rejecting | Before rejecting | After rejecting | Before rejecting | After rejecting | Before rejecting | After rejecting | Before rejecting | After rejecting |
| 1 | 9 | 7.75 | 7 | 6.5 | 5.5 | 4 | 4 | 2.5 | 2 | 0 | 2 | 0 | 2 | 0 | 2 | 0 | 2 | 0 |
| 25 | 7.75 | 8.25 | 8 | 8 | 7.5 | 6.5 | 4 | 0 | 0 | 0 | 0 | 0 | 0 | 0 | 0 | 0 | 0 | 0 |
| 50 | 9 | 8.5 | 8.5 | 9 | 8 | 8 | 4.75 | 0.5 | 0 | 0 | 0 | 0 | 0 | 0 | 0 | 0 | 0 | 0 |
| $K$ | 1.409 | 1.346 | 1.283 | 1.295 | 0.505 | 1.315 | 1.412 | 1.380 | 1.414 | 0 | 1.414 | 0 | 1.414 | 0 | 1.414 | 0 | 1.414 | 0 |

**Table E**
Readings at level $h = 40$ cm.

| Time $t$ [s] | $V_y$ [mm/s] for the distance from the left wall $x$ [cm] | | | | | | | | | | | | | | | | | | |
|---|---|---|---|---|---|---|---|---|---|---|---|---|---|---|---|---|---|---|---|
| | 0 | | 1 | | 2 | | 3 | | 4 | | 5 | 6 | 7 | 8 | 9 | 10 | 11 | 12 | 13 |
| | Before rejecting | After rejecting | Before rejecting | After rejecting | Before rejecting | After rejecting | Before rejecting | After rejecting | Before rejecting | After rejecting | | | | | | | | | |
| 1 | 1 | 0 | 2.5 | 0 | 3 | 0 | 4 | 0 | 5 | 0 | 5.75 | 6.5 | 6.5 | 7.5 | 8 | 8.25 | 9 | 8.75 | 8.5 |
| 25 | 0 | 0 | 0 | 0 | 0 | 0 | 0 | 0 | 0 | 0 | 0.25 | 2 | 6.25 | 6.25 | 6.75 | 6.75 | 6.75 | 6.5 | 7.25 |
| 50 | 0 | 0 | 0 | 0 | 0 | 0 | 0 | 0 | 0.25 | 0 | 0.25 | 2.5 | 3.75 | 5 | 7 | 7.75 | 8 | 8.25 | 9 |
| $K$ | 1.422 | 0 | 1.416 | 0 | 1.415 | 0 | 1.416 | 0 | 1.526 | 0 | 1.412 | 1.405 | 1.409 | 1.224 | 1.329 | 1.33 | 1.272 | 1.378 | 1.41 |

$\alpha = 0.05$, $K_{kr} = 1.412$.

**Table E** (*continued*)
Readings at level $h = 40$ cm.

| Time $t$ [s] | $V_y$ [mm/s] for the distance from the left wall $x$ [cm] | | | | | | | | | | | | | | | | | |
|---|---|---|---|---|---|---|---|---|---|---|---|---|---|---|---|---|---|---|
| | 14 | 15 | 16 | 17 | 18 | 19 | 20 | 21 | 22 | | 23 | | 24 | | 25 | | 26 | |
| | | | | | | | | | Before rejecting | After rejecting | Before rejecting | After rejecting | Before rejecting | After rejecting | Before rejecting | After rejecting | Before rejecting | After rejecting |
| 1 | 7.25 | 7.25 | 7 | 6.5 | 6 | 5 | 4 | 3.25 | 3.25 | 0 | 3.4 | 0 | 2.75 | 0 | 2.75 | 0 | 2.75 | 0 |
| 25 | 6.5 | 6.5 | 6.5 | 7 | 7 | 6 | 3 | 0 | 0 | 0 | 0 | 0 | 0 | 0 | 0 | 0 | 0 | 0 |
| 50 | 8.75 | 8.75 | 8.75 | 8.5 | 7.75 | 6.5 | 5.5 | 2 | 0 | 0 | 0 | 0 | 0 | 0 | 0 | 0 | 0 | 0 |
| $K$ | 1.359 | 1.337 | 1.378 | 1.376 | 1.283 | 1.33 | 1.293 | 1.307 | 2.386 | 0 | 2.386 | 0 | 1.414 | 0 | 1.414 | 0 | 1.414 | 0 |

**Table F**
Statistical values for calculations the confidence interval for level $h = 5$ cm.

| Distance from the left wall $x$ [cm] Statistical values | 8 | 9 | 10 | 11 | 12 | 13 | 14 | 15 | 16 | 17 |
|---|---|---|---|---|---|---|---|---|---|---|
| $\overline{V}_y$ | 0.2 | 1.4 | 4.2 | 9.8 | 16.2 | 16.3 | 15.6 | 10.9 | 6.3 | 1.8 |
| $S$ | 0.187 | 1.319 | 2.227 | 2.04 | 1.939 | 2.04 | 5.678 | 3.747 | 3.28 | 1.166 |
| $\overline{V}_y - t_{n-1,1-\frac{\alpha}{2}}\frac{S}{\sqrt{n-1}}$ | 0 | 0 | 1.11 | 6.97 | 13.51 | 13.47 | 7.72 | 5.70 | 1.75 | 0.18 |
| $\overline{V}_y + t_{n-1,1-\frac{\alpha}{2}}\frac{S}{\sqrt{n-1}}$ | 0.46 | 3.23 | 7.29 | 12.63 | 18.89 | 19.13 | 23.48 | 16.10 | 10.85 | 3.42 |

$n = 5, \alpha = 0.05, t_{n-1,1-\frac{\alpha}{2}} = 2.776.$

**Table G**
Statistical values to calculate the confidence interval for level $h = 10$ cm.

| Distance from the left wall $x$ [cm] Statistical values | 7 | 8 | 9 | 10 | 11 | 12 | 13 | 14 | 15 | 16 | 17 | 18 | 19 |
|---|---|---|---|---|---|---|---|---|---|---|---|---|---|
| $\overline{V}_y$ | 0.35 | 1.0 | 5.7 | 8.3 | 11.2 | 12.7 | 13.55 | 13.3 | 11.55 | 1.03 | 8.25 | 3.1 | 0.4 |
| $S$ | 0.374 | 0.707 | 3.572 | 2.821 | 1.166 | 1.749 | 2.629 | 2.686 | 1.584 | 1.939 | 1.677 | 2.154 | 0.374 |
| $n$ | 5 | 5 | 5 | 5 | 5 | 5 | 5 | 5 | 5 | 5 | 4 | 5 | 5 |
| $\overline{V}_y - t_{n-1,1-\frac{\alpha}{2}}\frac{S}{\sqrt{n-1}}$ | 0.17 | 0 | 0.74 | 4.38 | 9.58 | 10.27 | 9.90 | 9.57 | 9.41 | 7.61 | 5.17 | 0.11 | 0 |
| $\overline{V}_y + t_{n-1,1-\frac{\alpha}{2}}\frac{S}{\sqrt{n-1}}$ | 0.87 | 2.30 | 10.66 | 12.22 | 12.82 | 15.13 | 17.20 | 17.03 | 13.69 | 12.99 | 11.33 | 6.09 | 0.92 |

$n = 5, \alpha = 0.05, t_{4,\ 0{,}975} = 2.776, t_{3,\ 0{,}975} = 3.182.$

**Table H**
Statistical values to calculate the confidence interval for level $h = 20$ cm.

| Distance from the left wall $x$ [cm] Statistical values | 8 | 9 | 10 | 11 | 12 | 13 | 14 | 15 | 16 | 17 | 18 | 19 | 20 |
|---|---|---|---|---|---|---|---|---|---|---|---|---|---|
| $\overline{V}_y$ | 4 | 6.9 | 8.9 | 9.6 | 9.9 | 10.1 | 10.0 | 9.9 | 9.5 | 8.4 | 6.8 | 4.5 | 0.8 |
| $S$ | 2.236 | 1.629 | 0.893 | 0.451 | 0.37 | 0.325 | 0.306 | 0.515 | 0.707 | 1151 | 1.652 | 1.18 | 0.685 |
| $\overline{V}_y - t_{n-1,1-\frac{\alpha}{2}}\frac{S}{\sqrt{n-1}}$ | 0 | 3.91 | 7.26 | 8.8 | 9.22 | 9.5 | 9.44 | 8.95 | 8.2 | 6.33 | 3.77 | 2.33 | 0 |
| $\overline{V}_y + t_{n-1,1-\frac{\alpha}{2}}\frac{S}{\sqrt{n-1}}$ | 8.11 | 9.89 | 10.54 | 10.43 | 10.58 | 10.7 | 10.56 | 10.85 | 10.8 | 10.73 | 9.83 | 6.67 | 2.06 |

$n = 4, \alpha = 0.05, t_{n-1,\ 1-\frac{\alpha}{2}} = 3.182.$

**Table I**
Statistical values to calculate the confidence interval for level $h = 30$ cm.

| Distance from the left wall $x$ [cm] Statistical values | 5 | 6 | 7 | 8 | 9 | 10 | 11 | 12 | 13 | 14 | 15 | 16 | 17 | 18 | 19 | 20 | 21 |
|---|---|---|---|---|---|---|---|---|---|---|---|---|---|---|---|---|---|
| $\overline{V}_y$ | 1.8 | 2.1 | 2.4 | 5.5 | 7.4 | 7.8 | 8.3 | 8.4 | 8.3 | 8.6 | 8.2 | 7.9 | 7.8 | 7 | 6.2 | 6.3 | 1 |
| $S$ | 2.248 | 2.6 | 2.336 | 0.408 | 0.425 | 0.312 | 0.632 | 0.656 | 0.624 | 0589 | 0.312 | 0.217 | 1.027 | 1.08 | 1.65 | 0.354 | 1.08 |
| $\overline{V}_y - t_{n-1,1-\frac{\alpha}{2}}\frac{S}{\sqrt{n-1}}$ | 0 | 0 | 0 | 4.26 | 6.11 | 6.85 | 6.38 | 7.31 | 6.4 | 6.99 | 7.25 | 5.72 | 4.68 | 3.71 | 1.18 | 3.22 | 0 |
| $\overline{V}_y + t_{n-1,1-\frac{\alpha}{2}}\frac{S}{\sqrt{n-1}}$ | 8.73 | 10.01 | 9.6 | 6.74 | 8.69 | 8.75 | 10.22 | 9.89 | 10.2 | 10.21 | 9.15 | 10.08 | 10.92 | 10.29 | 10.22 | 5.38 | 4.29 |

$n = 3, \alpha = 0.05, t_{n-1,\ 1-\frac{\alpha}{2}} = 4.303.$

**Table J**
Statistical values to calculate the confidence interval for level $h = 40$ cm.

| Distance from the left wall $x$ [cm] Statistical values | 5 | 6 | 7 | 8 | 9 | 10 | 11 | 12 | 13 | 14 | 15 | 16 | 17 | 18 | 19 | 20 | 21 |
|---|---|---|---|---|---|---|---|---|---|---|---|---|---|---|---|---|---|
| $\overline{V}_y$ | 2.2 | 3.7 | 5.5 | 6.3 | 7.3 | 7.6 | 7.9 | 7.8 | 8.25 | 7.5 | 7.5 | 7.4 | 7.3 | 6.9 | 5.8 | 4.2 | 1.8 |
| $S$ | 2.536 | 2.014 | 1.242 | 1.021 | 0.54 | 0.624 | 0.52 | 0.965 | 0.736 | 0935 | 0.935 | 0.965 | 0.85 | 0.77 | 0.624 | 1.024 | 1.339 |
| $\overline{V}_y - t_{n-1,1-\frac{\alpha}{2}}\frac{S}{\sqrt{n-1}}$ | 0 | 0 | 1.72 | 3.19 | 5.66 | 5.7 | 6.15 | 6.7 | 6.72 | 7.46 | 6.43 | 6.33 | 6.33 | 6.08 | 5.08 | 3.03 | 0.27 |
| $\overline{V}_y + t_{n-1,1-\frac{\alpha}{2}}\frac{S}{\sqrt{n-1}}$ | 9.92 | 9.83 | 9.28 | 9.41 | 8.94 | 9.5 | 9.65 | 8.9 | 8.88 | 9.14 | 8.57 | 8.47 | 8.27 | 7.72 | 6.52 | 5.37 | 3.53 |

$n = 3, \alpha = 0.05, t_{n-1,\ 1-\frac{\alpha}{2}} = 4.303.$

**Table K**
Values of statistics from formulas (5) and (6) with using data from Tables A–E.

| $n_i$ | $13 - n_i = x_i$ | $13 + n_i = x_i$ | Time $t$ for levels $h$ [cm] | | | | |
|---|---|---|---|---|---|---|---|
| | | | 5 | 10 | 20 | 30 | 40 |
| 1 | 12 | 14 | 0.200 | 0.374 | 0.36 | 0 | 0.583 |
| 2 | 11 | 15 | 0.451 | 0.356 | 1.519 | 0.197 | 0.431 |
| 3 | 10 | 16 | 1.280 | 1.169 | 1.825 | 0.434 | 0.246 |
| 4 | 9 | 17 | 0.454 | 1.161 | 1.373 | 1.222 | 0 |
| 5 | 8 | 18 | | 1.651 | 1.744 | 1.838 | 0.68 |
| 6 | 7 | 19 | | 0.189 | | 3.179 | 0.305 |
| 7 | 6 | 20 | | | | 4.454[x] | 0.313 |
| 8 | 5 | 21 | | | | 0.454[x] | 0.296 |
| $t_{cr:0.05:n_{13-n_i}+n_{13+n_i}-2}$ | | | 2.306 | 2.306 | 2.447 | 2.447 | 2.776 |

**Table I.**
Statistical data for determining the stagnant zone boundaries.

| Height $h$ [cm] | Parameters of regression values $x_1$ $x_2$ | Time $t$ [s] | | | | | | | | | | | |
|---|---|---|---|---|---|---|---|---|---|---|---|---|---|
| | | 1 | | | | 25 | | | | 50 | | | |
| | | $x$ | $V_y$ | $x$ | $V_y$ | $x$ | $V_y$ | $x$ | $V_y$ | $x$ | $V_y$ | $x$ | $V_y$ |
| 1 | 2 | 3 | 4 | 5 | 6 | 7 | 8 | 9 | 10 | 11 | 12 | 13 | 14 |
| 5 | | 8 | 0.25 | 14 | 26 | 9 | 0 | 14 | 16 | 9 | 0.5 | 14 | 13 |
| | | 9 | 0.5 | 15 | 7 | 10 | 2 | 15 | 17 | 10 | 6 | 15 | 12.5 |
| | | 10 | 1 | 16 | 1 | 11 | 10 | 16 | 6 | 11 | 12 | 16 | 11 |
| | | 11 | 6 | 17 | 0.5 | 12 | 14 | 17 | 0.5 | 12 | 18 | 17 | 2.5 |
| | $a$ | −14.93 | | | | −46.0 | | 9.9 | | −52.3 | | 60.9 | |
| | $b$ | 1.775 | | | | 5.0 | | −5.75 | | 5.83 | | −3.30 | |
| | $A$ | | | −122.11 | | | | | | | | | |
| | $B$ | | | 2015.8 | | | | | | | | | |
| | $r$ | 0.841 | | 0.915 | | 0.977 | | −0.930 | | 0.998 | | −0.868 | |
| | $x_1$ $x_2$ | 8.41 | | 16.51 | | 9.2 | | 17.22 | | 8.94 | | 18.45 | |
| 10 | | 8 | 1 | 15 | 13 | 8 | 0 | 16 | 10 | 7 | 0 | 16 | 13 |
| | | 9 | 3 | 16 | 8 | 9 | 0.5 | 17 | 6 | 8 | 1 | 17 | 9 |
| | | 10 | 6 | 18 | 1 | 10 | 4 | 18 | 0.5 | 9 | 6 | 18 | 3 |
| | | 11 | 10 | 19 | 0 | 11 | 13 | 19 | 0 | 10 | 10 | 19 | 0.5 |
| | $a$ | −23.5 | | | | −36.0 | | | | −25.5 | | | |
| | $b$ | 3.00 | | | | 4.25 | | | | 3.5 | | | |
| | $A$ | | | −50.84 | | | | −58.35 | | | | −69.63 | |
| | $B$ | | | 949.47 | | | | 1088.85 | | | | 1324.68 | |
| | $r$ | 0.989 | | 0.991 | | 0.912 | | 0.971 | | 0.973 | | 0.992 | |
| | $x_1$ $x_2$ | 7.83 | | 18.68 | | 8.47 | | 18.66 | | 7.29 | | 19.02 | |
| 20 | | 7 | 0 | 18 | 4.5 | 7 | 0 | 17 | 9.5 | 7 | 0 | 18 | 8.5 |
| | | 8 | 5 | 19 | 3 | 8 | 1 | | | | | | |
| | | 9 | 5.5 | 20 | 1.75 | 9 | 5 | 19 | 4 | 9 | 8 | 20 | 0.25 |
| | | 10 | 8 | 21 | 0 | 10 | 8 | 20 | 0 | 10 | 9.5 | 21 | 0 |
| | $a$ | | | 31.075 | | | | 66.03 | | | | | |
| | $b$ | | | −1.475 | | | | −3.28 | | | | | |
| | $A$ | 25.53 | | | | 26.35 | | | | 33.23 | | −57.42 | |
| | $B$ | −174.54 | | | | −190.83 | | | | −234.68 | | 1187.58 | |
| | $r$ | −0.963 | | −0.998 | | −0.955 | | −0.978 | | −0.986 | | 0.957 | |
| | $x_1$ $x_2$ | 6.84 | | 21.07 | | 7.24 | | 20.16 | | 7.06 | | 20.68 | |
| 30 | | 4 | 0 | 19 | 4 | 6 | 0 | 18 | 7.5 | 4 | 0 | 19 | 8 |
| | | 5 | 5 | 20 | 4 | 7 | 0.5 | 19 | 6.5 | 5 | 0.5 | 20 | 4.75 |
| | | 6 | 5.75 | 21 | 2.5 | 8 | 5.5 | 20 | 4 | 6 | 0.5 | 21 | 0.5 |
| | | 7 | 5.75 | 22 | 0 | 9 | 7.25 | 21 | 0 | 7 | 1 | 22 | 0 |
| | $a$ | | | 30.30 | | −16.75 | | 53.25 | | −1.15 | | | |
| | $b$ | | | −1.35 | | 2.675 | | −2.50 | | 0.30 | | | |
| | $A$ | 14.50 | | | | | | | | | | −54.91 | |
| | $B$ | −54.63 | | | | | | | | | | 1190.09 | |
| | $r$ | −0.915 | | −0.923 | | 0.956 | | −0.966 | | 0.949 | | 0.972 | |
| | $x_1$ $x_2$ | 3.77 | | 22.44 | | 6.26 | | 21.3 | | 3.83 | | 21.67 | |
| 40 | | 4 | 0 | 19 | 5 | 4 | 0 | 18 | 7 | 4 | 0 | 19 | 6.5 |
| | | 5 | 5.75 | 20 | 4 | 5 | 0.25 | 19 | 6 | 5 | 0.5 | 20 | 5.5 |
| | | 6 | 6.5 | 21 | 3.25 | 6 | 2 | 20 | 3 | 6 | 2.5 | 21 | 2 |
| | | 7 | 6.5 | 22 | 0 | 7 | 6.25 | 21 | 0 | 7 | 3.75 | 22 | 0 |
| | $a$ | | | 35.35 | | −9.15 | | 50.8 | | −5.60 | | 50.65 | |
| | $b$ | | | −1.575 | | 2.05 | | −2.40 | | 1.325 | | −2.30 | |
| | $A$ | 16.38 | | | | | | | | | | | |
| | $B$ | −61.601 | | | | | | | | | | | |
| | $r$ | −0.909 | | −0.940 | | 0.916 | | −0.980 | | 0.978 | | −0.981 | |
| | $x_1$ $x_2$ | 3.76 | | 22.44 | | 4.46 | | 21.17 | | 4.23 | | 22.02 | |

## References


[1] I. Sielamowicz, M. Czech, T.A. Kowalewski, Empirical description of flow parameters in eccentric flow inside a silo model, Powder Technol. 198 (2010) 381–394.
[2] I. Sielamowicz, M. Czech, T.A. Kowalewski, Empirical analysis of eccentric flow registered by the DPIV technique inside a silo model, Powder Technol. 212 (2011) 38–56.
[3] ENV 1991, Part 4 Eurocode 1, Basis of Design and Actions on Structures. Part 4 Actions on Silos and Tanks Brussels Belgium, 1995.
[4] ACI 313, Alternate Design Procedure, Discussion Document Before ACI Committee 313 on Concrete Bins, Silos and Bunkers for Storing Granular Materials, ACI, Detroit, 1989.
[5] ASAE EP433, Loads Exerted by Free-flowing Grains on Bins, ASAE Engineering Practice EP433 ASAE Standards, 1997.
[6] J.M. Rotter, Guide for the Economic Design of Metal Silos, E&FN Spon, London, 1998.
[7] F. Ayuga, M. Guaita, P.J. Aguado, A. Couto, Discharge and the eccentricity of the hopper influence on the silo wall pressures, J. Eng. Mech. 127 (10) (2001) 1067–1074.
[8] G.E. Blight, Eccentric discharge of a large coal bin with six outlets, Bulk Solids Handl. 11 (2) (1991) 451–457.
[9] J.M. Rotter, The analysis of steel bins subject to eccentric discharge, Proc., 2nd Inter. Conference on Bulk Materials Storage Handling and Transportation, Ins. of Eng. Wollongong, Australia July, 1986, pp. 264–271.
[10] J.W. Carson, Silo failures: case histories and lessons learned, Third Israeli Conference for Conveying and Handling of Particulate Solids, Dead Sea Israel, May 2000.
[11] C.S. Chou, Y.C. Chuang, J. Smid, S.S. Hsiau, J.T. Kuo, Flow patterns and stresses on the wall in a moving granular bed with eccentric discharge, Adv. Powder Technol. 13 (1) (2002) 1–13.
[12] C.S. Chou, J.Y. Hsu, Kinematic model for granular flow in a two-dimensional flat bottomed hopper, Adv. Powder Technol. 14 (3) (2003) 313–331.
[13] M. Molenda, J. Horabik, S.A. Thompson, I.J. Ross, Bin loads induced by eccentric filling and discharge of grain, Trans. ASAE 45 (3) (2002) 781–785.
[14] R.M. Nedderman, U. Tüzün, A kinematic model for the flow of granular materials, Powder Technol. 22 (1979) 243–253.
[15] J.S. Guaita, A. Couto, F. Ayuga, Numerical simulation of wall pressure during discharge of granular material from cylindrical silos with eccentric hoppers, Biosyst. Eng. 85 (1) (2003) 101–109.
[16] C.Y. Song, J.G. Teng, Buckling of circular steel silos subject to code-specified eccentric discharge pressures, Eng. Struct. 25 (2003) 1397–1417.
[17] K. Nübel, W. Huang, A study of localized deformation pattern in granular media, Comput. Methods Appl. Mech. Eng. 193 (2004) 2719–2743.

[18] J.F. Chen, J.M. Rotter, J.Y. Ooi, Z. Zhong, Flow patterns measurement in a full scale silo containing iron ore, Chem. Eng. Sci. 60 (2005) 3029–3041.
[19] J. Nielsen, V. Askegaard, Scale errors in model tests in granular media with special reference to silo models, Powder Technol. 16 (1) (1977) 123–130.
[20] H.E. Wright, G.F. Cudahy, J.T. Van Kuren, Degradation of laser beam by a two dimensional turbulent jet, AIAA J. 17 (10) (1979) 1091–1097.
[21] J. Nielsen, N.O. Kristiansen, Related measurements of pressure condition in full scale barley silo and in silo model, Proc. of the International Conference on Design of Silos for Strength and Flow, University of Lancaster, Powder Advisory Centre, September 1980.
[22] J. Munch-Andersen, J. Nielsen, Size effects in large grain silos, Bulk Solids Handl. 6 (1986) 885–889.
[23] J. Nielsen, Pressures from flowing granular solids in silos, Philos. Trans. R. Soc. Lond. Ser. A 356 (1747) (1998) 2667–2684.
[24] J.F. Chen, J.M. Rotter, J.Y. Ooi, A review of numerical prediction methods for silo wall pressures, Adv. Struct. Eng. 2 (2) (1999) 119–135.
[25] J.F. Chen, K.F. Zhang, J.Y. Ooi, J.M. Rotter, Visualisation of solids flow in a full scale silo, Proc., 3rd European Symposium on Storage and Flow of Particulate Solids (Janssen Centennial), Nuremberg, Germany, 21–23 March, 1995, pp. 427–436.
[26] J.F. Chen, Interpretation of Flow and Pressures in Full Scale Silos(Ph.D. Thesis) University of Edinburg, 1996. (678 pp.).
[27] A. Medina, J.A. Cordova, E. Luna, C. Treviño, Velocity filed measurements in granular gravity flow, Phys. Lett. A 250 (1998) 111–116.
[28] R.M. Lueptow, A. Akonur, T. Shinbrot, PIV for granular flow, Exp. Fluids 28 (2) (2000) 183–186.
[29] A.J. Waters, A. Drescher, Modelling plug flow in bins/hoppers, Powder Technol. 113 (2000) 168–175.
[30] M. Ostendorf, J. Schwedes, Application of particle image velocimetry for velocity measurements during silo discharge, Powder Technol. 158 (2005) 69–75.
[31] J.U. Böhrnsen, H. Antes, M. Ostendorf, J. Schwedes, Silo discharge: measurement and simulation of dynamic behaviour in bulk solids, Chem. Eng. Technol. 27 (2004) 71–76.
[32] I. Sielamowicz, S. Błoński, T.A. Kowalewski, Optical technique DPIV in measurements of granular material flow, part 1 of 3—plane hoppers, Chem. Eng. Sci. 60 (2) (2005) 589–598.
[33] I. Sielamowicz, S. Błoński, T.A. Kowalewski, Optical technique DPIV in measurements of granular material flow, part 2 of 3 — converging hoppers, Chem. Eng. Sci. 61 (2006) 5307–5317.
[34] I. Sielamowicz, Experimental analysis of granular material flows using the technique of digital particle image velocimetry, Eng. Trans. 53 (2) (2005) 195–227.
[35] D.A. Steingart, J.W. Evans, Measurements of granular flow in two-dimensional hoppers by particle image velocimetry. Part I: experimental method and results, Chem. Eng. Sci. 60 (2005) 1043–1051.
[36] P.M. Blair-Fish, P.L. Bransby, Flow Patterns and Wall Stresses in a Mass-Flow Bunker, 1973. 17–26 (Error! Not a valid link).
[37] A. Drescher, T.W. Cousens, P.L. Bransby, Kinematics of the mass flow of granular material through a plane hopper, Geotechnique 28 (1) (1978) 27–42.
[38] J.Y. Ooi, J.F. Chen, J.M. Rotter, Measurement of solids flow patterns in a gypsum silo, Powder Technol. 99 (3) (1998) 272–284.
[39] J. Choi, A. Kudrolli, M.Z. Bazant, Velocity profile of granular flow inside silos and hoppers, J. Phys. Condens. Matter 17 (2005) S2533–S2548.
[40] C.S. Chou, J.Y. Hsu, Y.D. Lau, Flow patterns and stresses on the wall in a two-dimensional flat-bottomed bin, J. Chin. Inst. Eng. Trans. Chin. Inst. Eng. Ser. A 26 (4) (2003) 397–408.
[41] H. de Clercq, Investigation into stability of a silo with concentric and eccentric discharge, Civ. Eng. S. Afr. 32 (3) (1990) 103–107.
[42] M. Wójcik, G.G. Enstad, M. Jecmenica, Numerical calculations of wall pressures and stresses in steel cylindrical silos with concentric and eccentric hoppers, J. Part. Sci. Technol. 21 (3) (2003) 247–258.
[43] G.M. Quenot, J. Pakleza, T.A. Kowalewski, Particle image velocimetry with optical flow, Exp. Fluids 25 (1998) 177–189.
[44] I. Likiesh, J. Liaga, Osnownyje tablicy matiematiczeskoj statistiki, Moskwa, 1985.
[45] W. Volk, Applied Statistics for Engineers, second edition McGraw-Hill, 1979.